© 2014. Published by The Company of Biologists Ltd | Journal of Cell Science (2014) 127, 158–171 doi:10.1242/jcs.134270

RESEARCH ARTICLE

Epithelial–mesenchymal status influences how cells deposit fibrillin microfibrils

Andrew K. Baldwin[1,*], Stuart A. Cain[1,*], Rachel Lennon[1,2], Alan Godwin[1], Catherine L. R. Merry[3] and Cay M. Kielty[1,‡]

ABSTRACT

Here, we show that epithelial–mesenchymal status influences how cells deposit extracellular matrix. Retinal pigmented epithelial (RPE) cells that expressed high levels of E-cadherin and had cell–cell junctions rich in zona occludens (ZO)-1, β-catenin and heparan sulfate, required syndecan-4 but not fibronectin or protein kinase C α (PKCα) to assemble extracellular matrix (fibrillin microfibrils and perlecan). In contrast, RPE cells that strongly expressed mesenchymal smooth muscle α-actin but little ZO-1 or E-cadherin, required fibronectin (like fibroblasts) and PKCα, but not syndecan-4. Integrins α5β1 and/or α8β1 and actomyosin tension were common requirements for microfibril deposition, as was heparan sulfate biosynthesis. TGFβ, which stimulates epithelial–mesenchymal transition, altered gene expression and overcame the dependency on syndecan-4 for microfibril deposition in epithelial RPE cells, whereas blocking cadherin interactions disrupted microfibril deposition. Renal podocytes had a transitional phenotype with pericellular β-catenin but little ZO-1; they required syndecan-4 and fibronectin for efficient microfibril deposition. Thus, epithelial–mesenchymal status modulates microfibril deposition.

KEY WORDS: Epithelial cell, Mesenchymal cell, Fibrillin-1, Fibronectin, Perlecan, Integrin, Syndecan, Cell–cell junction

INTRODUCTION

Fibrillin, the main component of microfibrils of the extracellular matrix (ECM), supports elastic fibre formation and controls transforming growth factor β (TGFβ) bioavailability (Baldwin et al., 2013; Ramirez and Sakai, 2010). Its importance is highlighted by mutations that cause Marfan syndrome (Ramirez and Dietz, 2009), and Weill–Marchesani and stiff skin syndromes (Faivre et al., 2003; Loeys et al., 2010). Although mechanisms of microfibril assembly and deposition are incompletely understood, in mesenchymal cultures the adhesive glycoprotein fibronectin (FN) is needed (Kinsey et al., 2008; Sabatier et al., 2009; Zilberberg et al., 2012). This relationship was unexpected, as fibrillin microfibrils arose in early metazoans but FN-like molecules only in chordates (Ozbek et al., 2010; Piha-Gossack et al., 2012; Tucker and Chiquet-Ehrismann, 2009).

Although FN is a regulator of ECM deposition (Sottile and Hocking, 2002), the underlying mechanism is unclear. ECM fibrillogenesis requires Arg-Gly-Asp (RGD) engagement of α5β1 integrin (Takahashi et al., 2007) and RhoA activation of Rho kinases, which regulate stress fibres, focal adhesions and cortical myosin (Singh et al., 2010; Yoneda et al., 2007), with cytoskeletal tension exposing FN self-assembly sites. Epithelial cadherin junctions can operate analogously to the focal adhesions of cultured mesenchymal cells, transferring to integrins the tension needed for FN fibrillogenesis (Dzamba et al., 2009). Fibrillin-1 can interact with FN, which could be a microfibril template (Hubmacher et al., 2011; Kinsey et al., 2008; Sabatier et al., 2009). However, microfibrils are deposited in FN-null cultures (Dallas et al., 2005). We have also shown that microfibril deposition needs FN RGD, α5β1 integrin and Rho kinase (Kinsey et al., 2008), implicating FN-induced cytoskeletal tension in fibrillin-1 assembly.

Heparan sulfate (HS) proteoglycans also influence microfibril assembly. Although FN and fibrillin-1 both bind HS (Cain et al., 2008; Ritty et al., 2003; Singh et al., 2010; Tiedemann et al., 2001), exogenous heparin, heparinase or β-D-xyloside block only microfibril deposition (Chung and Erickson, 1997; Ritty et al., 2003; Tiedemann et al., 2001). Syndecans 2 and 4, widely expressed transmembrane HS proteoglycans, are implicated in FN deposition. Syndecan-2 affects FN deposition by signalling (Klass et al., 2000) and sulfation (Galante and Schwarzbauer, 2007). Syndecan-4 binds FN, inducing the formation of focal adhesions (Gopal et al., 2010; Woods et al., 2000) and activation of Rho, Rac and protein kinase Cα (PKCα) (Bass et al., 2008; Dovas et al., 2006), yet syndecan-4-depleted cells deposit FN (Galante and Schwarzbauer, 2007). Mice null for syndecan-4 and syndecan-1 have wound healing phenotypes, implying compensatory effects; syndecan-1 is also implicated in epithelial–mesenchymal transition (EMT) (Couchman, 2010; Masola et al., 2012; Stepp et al., 2007). Perlecan, a basement membrane component, binds fibrillin-1 and FN through protein and HS interactions (Cain et al., 2006; Hopf et al., 2001; Tiedemann et al., 2005).

Although most mesenchymal cells deposit abundant fibrillin microfibrils, only certain epithelial cells express fibrillin-1 (Dzamba et al., 2001; Haynes et al., 1997; Ritty et al., 2003). Here, we have investigated deposition of microfibrils and perlecan in human retinal pigmented epithelial (ARPE-19) cells, a model of microfibril deposition (Boregowda et al., 2012; Massam-Wu et al., 2010; Nonaka et al., 2009; Wachi et al., 2005), and in podocytes, which are specialised glomerular epithelial cells (Lennon et al., 2013). Both of these cell types

[1]Wellcome Trust Centre for Cell-Matrix Research, Faculty of Life Sciences, University of Manchester, Manchester M13 9PT, UK. [2]Faculty of Medical and Human Sciences, University of Manchester, Manchester M13 9PT, UK. [3]Faculty of Engineering and Physical Sciences, University of Manchester, Manchester M13 9PT, UK.
*These authors contributed equally to this work

‡Author for correspondence (cay.kielty@manchester.ac.uk)

Received 30 April 2013; Accepted 4 October 2013

Journal of Cell Science

Journal of Cell Science (2014) 127, 158–171 doi:10.1242/jcs.134270

contribute to elastic-fibre-containing membranes *in vivo* (Bruch's membrane; glomerular basement membrane). We show that cells in distinct epithelial–mesenchymal states have different dependencies on FN, syndecan-4 and PKCα for microfibril deposition, that cadherins modulate microfibril deposition, and that α5β1 and α8β1 integrins, cytoskeletal tension and HS are essential for the process.

RESULTS

We investigated the differences and similarities in the deposition of fibrillin microfibrils and perlecan between epithelial cells and adult human dermal fibroblasts (HDFs). Initial epithelial experiments used ARPE-19 cells (designated ARPE-19A) from the American Tissue Culture Collection (batch 58280268). Subsequent experiments compared ARPE-19A cells with additional cultures (batch 59270158, designated ARPE-19B, and batch 60279299, designated ARPE-19C). We also assessed human podocytes for dependence of microfibril deposition on FN and syndecan-4. HaCaT and human mammary epithelial cells (MCF10A) did not deposit detectable microfibrils (data not shown).

ARPE-19A cells do not require FN for microfibril deposition

We and others have shown that depletion of FN in fibroblasts (Kinsey et al., 2008; Sabatier et al., 2009) blocks deposition of fibrillin microfibrils. To investigate whether FN is indispensable for microfibril deposition by other cell types, we compared ARPE-19A cells with HDFs (Fig. 1A; supplementary material Fig. S1A,B).

Real-time quantitative PCR (qPCR) analysis of expression of mRNA encoding fibrillin-1 and FN in ARPE-19A and HDF cells revealed that ARPE-19A cells expressed 1.4-fold more fibrillin-1 than FN, whereas HDFs expressed 8.3-fold more FN than fibrillin-1 (supplementary material Fig. S2Ai,iv). FN was depleted from ARPE-19A cells or HDFs for up to 8 days by siRNA treatment repeated every 48 hours, to ensure maximal knockdown (>98% in both ARPE-19A and HDF cultures) (supplementary material Fig. S3A,C). Western blotting of medium and cell layer extracts of knockdown cultures revealed reduced levels of extracellular fibrillin-1 (Fig. 1D).

In control and FN-depleted ARPE-19A cultures, microfibrils were detected by immunostaining (with the anti-fibrillin-1 antibody HPA021057 (Fig. 1A) and also antibody 11C1.3 (not shown) (see Fig. 8A, which shows that microfibril assembly occurs basally). Electron microscopy (EM) confirmed these results (Fig. 1C). Thus, unlike HDFs, ARPE-19A cells did not depend on FN expression for microfibril deposition. In contrast, FN depletion in adult HDFs blocked microfibril deposition (supplementary material Fig. S1), as reported previously (Kinsey et al., 2008; Sabatier et al., 2009).

ARPE-19B and ARPE-19C cells require FN for microfibril deposition

Given that the ability of ARPE-19A cells to deposit microfibrils when FN was depleted was unexpected, we tested independent batches of ARPE-19 cells (ARPE-19B, ARPE-19C), which were cultured in the same manner as ARPE-19A cells.

qPCR analysis revealed that ARPE-19B cells expressed comparable levels of fibrillin-1 and FN to ARPE-19A cells, with 1.7-fold more fibrillin-1 than FN (supplementary material Fig. S2Aii). FN was depleted from ARPE-19B cells by siRNA as above (99% knockdown) (supplementary material Fig. S3B). Western blotting of medium and cell layer extracts after FN knockdown revealed high levels of fibrillin-1 in medium (Fig. 1D). EM failed to detect microfibrils in FN-depleted ARPE-19B cultures (not shown). Immunofluorescence microscopy confirmed lack of microfibrils in FN-depleted ARPE-19B and ARPE-19C (99% knockdown) cultures (Fig. 1Bi,ii). Thus, FN is required for microfibril deposition by these cells, even though fibrillin-1 is expressed and secreted.

Supplementing control ARPE-19B cultures with cellular FN (cFN; 10 μg/ml) for 12 days (replaced every 48 hours, with repeated FN siRNA) enhanced abundance of microfibrils and FN (supplementary material Fig. S4). With FN-siRNA-treated ARPE-19B cells, cFN only slightly enhanced fibrillin-1 deposition (supplementary material Fig. S4).

Podocytes require FN for abundant microfibrils

qPCR analysis of proliferating podocytes revealed that they expressed higher levels of FN but lower levels of fibrillin-1 than ARPE-19 cultures (supplementary material Fig. S2Aiii). FN was depleted by siRNA, as above (98% knockdown) (supplementary material Fig. S3D). Western blotting, after FN knockdown, detected fibrillin-1 predominantly in medium (Fig. 1E). EM detected a few microfibrils in FN-depleted podocyte cultures but no arrays (Fig. 1C); immunofluorescence microscopy confirmed these findings (Fig. 1Biii,iv). Thus, although FN is not needed to assemble microfibrils, it greatly enhances their deposition.

ARPE-19 cells vary in dependency on FN for perlecan deposition, but do not require perlecan for FN or microfibril deposition

Perlecan is a component of basement membranes and mesenchymal matrices (Melrose et al., 2008). qPCR revealed that perlecan mRNA expression level was 2.5-fold less in ARPE-19A than in ARPE-19B cells; HDFs expressed abundant perlecan (supplementary material Fig. S2A). Immunofluorescence microscopy of FN-depleted cultures, as above, revealed that FN was required for deposition of perlecan by ARPE-19B cultures and HDFs, but not ARPE-19A cultures (supplementary material Fig. S5). Perlecan knockdown was performed to determine whether it influenced deposition of FN or microfibrils. Western blotting revealed that fibrillin-1 and FN were abundant in medium and cell layer extracts of perlecan-depleted ARPE-19A and ARPE-19B cultures (Fig. 1D). Immunofluorescence microscopy revealed that perlecan was not required for their deposition (supplementary material Fig. S5; and not shown).

ARPE-19 cells and podocytes vary in expression of epithelial–mesenchymal markers

We investigated why ARPE-19B but not ARPE-19A cultures required FN for microfibril and perlecan deposition, and why podocytes assembled a few microfibrils when FN was depleted yet required FN to deposit microfibril arrays. Because FN fibrillogenesis is regulated by focal adhesions (Singh et al., 2010) or by epithelial cell–cell junctions (Dzamba et al., 2009), and given that ARPE-19 cells can undergo EMT (Chen et al., 2012; Li et al., 2011; Tian et al., 2005), we assessed their EMT marker expression (Fig. 2).

Expression of transcription factors implicated in EMT was examined (Fig. 2; supplementary material Fig. S2B; Fig. S3D). There was lower expression of SNAI1 in ARPE-19B than ARPE-19A cells or podocytes. SNAI1 and SNAI2 can induce EMT (Kalluri and Weinberg, 2009). SNAI2 expression was high in podocytes and ARPE-19A cells but low in ARPE-19B cultures. TWIST1 expression was similar in all cultures. All cells

Journal of Cell Science (2014) 127, 158–171 doi:10.1242/jcs.134270

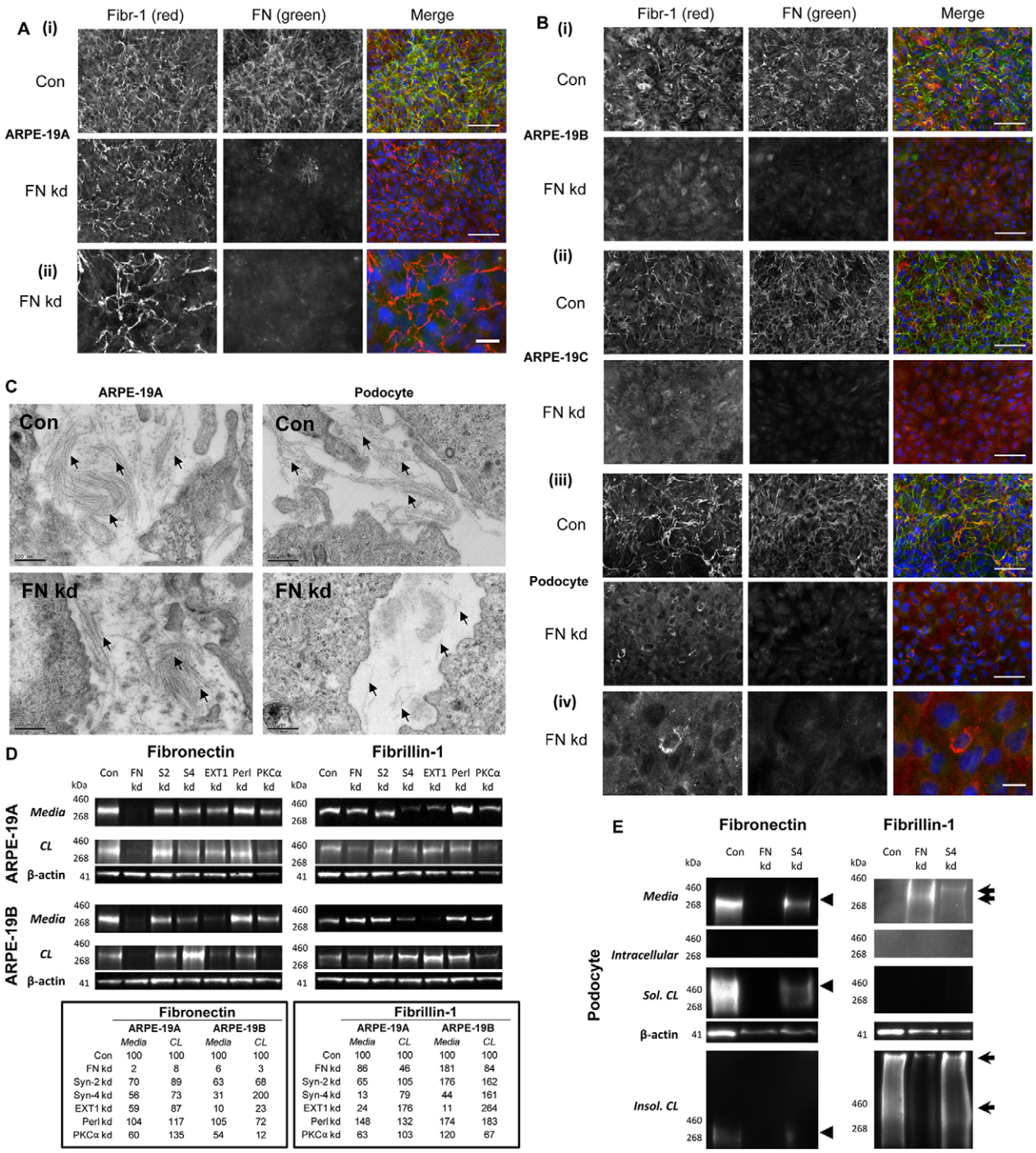

Fibronectin

	ARPE-19A		ARPE-19B	
	Media	*CL*	*Media*	*CL*
Con	100	100	100	100
FN kd	2	8	6	3
Syn-2 kd	70	89	63	68
Syn-4 kd	56	73	31	200
EXT1 kd	59	87	10	23
Perl kd	104	117	105	72
PKCα kd	60	135	54	12

Fibrillin-1

	ARPE-19A		ARPE-19B	
	Media	*CL*	*Media*	*CL*
Con	100	100	100	100
FN kd	86	46	181	84
Syn-2 kd	65	105	176	162
Syn-4 kd	13	79	44	161
EXT1 kd	24	176	11	264
Perl kd	148	132	174	183
PKCα kd	63	103	120	67

Fig. 1. ARPE-19A cells did not depend on FN for microfibril deposition. Immunofluorescence microscopy of (A) ARPE-19A cells and (B) ARPE-19B, ARPE-19C cells and podocytes (all after 7 days), showing deposition of fibrillin-1 (Fibr-1; black and white, red) and FN (black and white, green), with nuclei stained with DAPI (blue). Images were taken using a 20× objective. Specific band-pass filter sets for DAPI, FITC and Cy3 or Cy5 were used to prevent bleed-through. Control cultures (Con) showed partial colocalisation of fibrillin-1 and FN (yellow). (A) FN knockdown (kd) ARPE-19A cultures had microfibrils, shown at two magnifications [(i) and (ii)]; (B) FN kd ARPE-19B and ARPE-19C cultures had no detectable microfibrils. FN kd podocytes exhibited limited extracellular fibrillin-1 staining, shown at two magnifications [(iii) and (iv)]. Scale bars: 100 μm (Ai,Bi,Bii,Biii); 25 μm (Aii,Biv). Representative images from $n=5$ (A,Bi) or $n=3$ (Bii,Biii,Biv) experiments are shown. (C) Electron microscopy of 12-day ARPE-19A cell layers, showing extracellular microfibril bundles (black arrows) in control and FN kd cultures. Scale bars: 500 nm. (D) Medium and cell layer extracts from ARPE-19A and ARPE-19B cultures in control (Con) and knockdown (kd) experiments (FN, syndecan-2, syndecan-4, EXT1, perlecan or PKCα) were separated on 3–8% Tris-acetate gels in reducing conditions, and analyzed by western blotting for fibrillin-1 (antibody HPA021057) or FN (antibody FN-3E2), and β-actin (mAbAC-74; as a loading control for cell layer extracts). Molecular mass markers are indicated. Quantification of band intensity is shown as percentage of control band intensity (where Con=100%). Data shown are from a representative experiment, with biological and technical repeats exhibiting the same trends ($n=3$). (E) Medium and sequential intracellular (1% NP40 extraction) and cell layer (CL; soluble and insoluble) extracts from podocyte cultures in control (Con) and knockdown (kd) experiments (FN or syndecan-4) were separated on 3–8% Tris-acetate gels in reducing conditions, and analyzed by western blotting for fibrillin-1 (antibody HPA021057) or FN (antibody FN-3E2), and β-actin (mAbAC-74; as loading control for cell lysates). Molecular mass markers are indicated.

Journal of Cell Science (2014) 127, 158–171 doi:10.1242/jcs.134270

expressed mesenchymal markers [smooth muscle α-actin (SMA) and PDGF receptor-β].

We also analyzed cell–cell junction proteins in ARPE-19 cells and podocytes. After 7 days of culture, ARPE-19A cells expressed the highest levels of E-cadherin; N-cadherin levels were high in ARPE-19 cultures and podocytes (Fig. 2A; supplementary material Fig. S2B; Fig. S3D). Immunostaining of ZO-1 (also known as TJP1; antibody T11, clone R40.76) revealed that ARPE-19A cultures, but not ARPE-19B cultures or podocytes, had well-organised tight junctions (Fig. 2B). Western blotting for E-cadherin (antibody 24E10) confirmed that ARPE-19A cultures had higher levels of E-cadherin protein than ARPE-19B cells (Fig. 2C) or podocytes (not shown). Immunomicroscopy for E-cadherin showed punctate localisation most prominently in ARPE-19A cells, whereas N-cadherin and β-catenin localised at cell junctions in ARPE-19A cells and podocytes (Fig. 2D).

Thus, ARPE-19A cultures are the most epithelial on the basis of highest levels of E-cadherin, and cell–cell staining of ZO-1, β-catenin and N-cadherin. Podocytes appear to be transitional, with cell–cell staining but high levels of SNAI1 transcription factors. ARPE-19B cells are less epithelial on the basis of reduced E-cadherin and poorly defined cell–cell junctions.

Inhibition of cadherin junctions disrupt microfibril deposition

Dzamba et al. (Dzamba et al., 2009) have shown that cadherin junctions can regulate FN assembly in epithelial cells. A peptide inhibitor of cadherin interactions (A7) (Devemy and Blaschuk, 2009) disrupted microfibril assembly by ARPE-19A and ARPE-19B cultures, and FN formed only punctate arrays (Fig. 3). Thus, cadherin junctions influence microfibril deposition. When FN was depleted, only ARPE-19A cells deposited some microfibrils in the presence of the blocking peptide; in these cells, cadherin-blocking effects were FN independent.

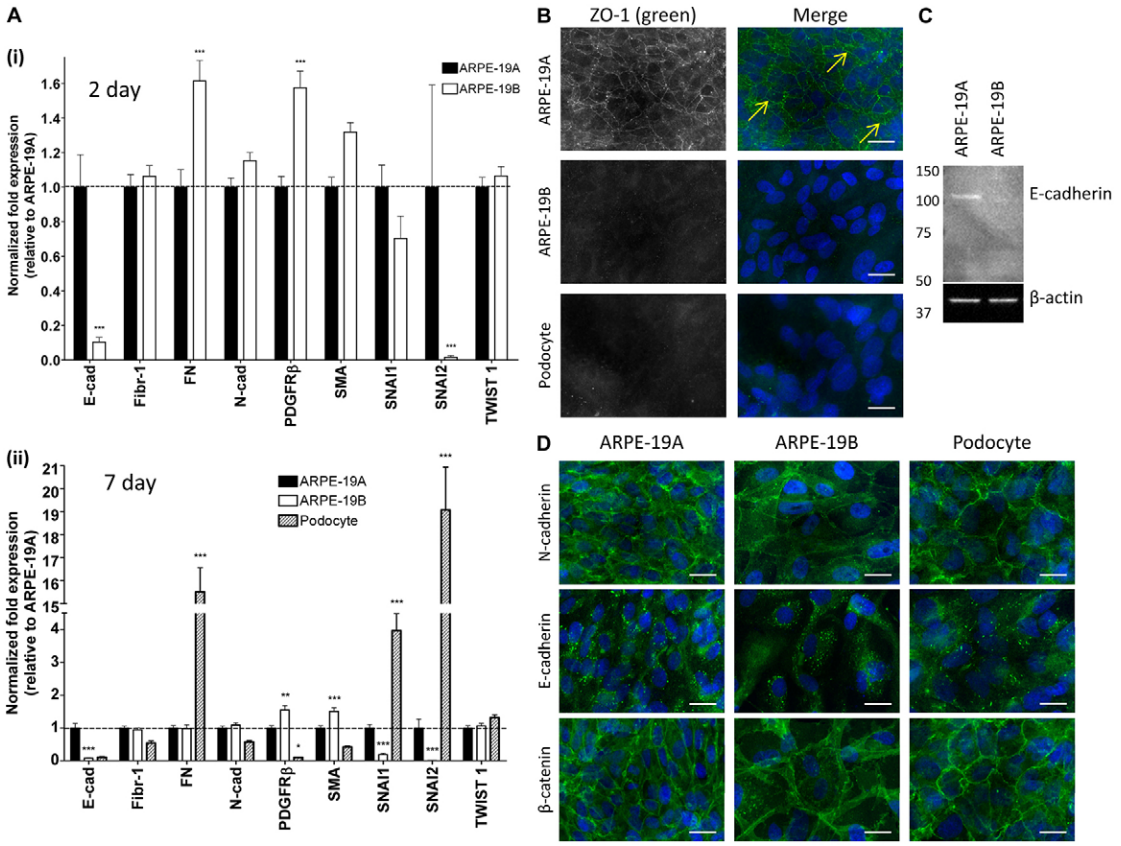

Fig. 2. ARPE-19A and ARPE-19B cultures differ in epithelial–mesenchymal status. (A) Real-time quantitative PCR (qPCR) analysis of gene expression of E-cadherin (E-cad), fibrillin-1 (Fibr-1), fibronectin (FN), N-cadherin (N-cad), PDGF receptor-β (PDGFRβ), smooth muscle α-actin (SMA), SNAI1, SNAI2 and TWIST1 in ARPE-19A and ARPE-19B cultures and podocytes after (i) 2 days (ARPE-19A and ARPE-19B only) and (ii) 7 days. E-cadherin expression is reduced in ARPE-19B cells at days 2 and 7. FN expression is increased in ARPE-19B cells at day 2, and SMA is increased at day 7. PDGFRβ expression is increased in ARPE-19B cultures at both time points. E-cadherin and PDGFRβ expression is lower in podocytes than ARPE-19A cells, with expression of FN, SNAI1 and SNAI2 higher in podocytes (day 7). Expression was normalised using a combination of GAPDH and TATA box binding protein (TBP) expression, and is reported relative to expression levels in ARPE-19A cultures (where ARPE-19A expression is set at 1). All data are represented as the mean±s.e.m. and analyzed by two-way ANOVA (ARPE-19A versus ARPE-19B and ARPE-19A versus podocyte). *$P<0.05$; **$P<0.01$; ***$P<0.001$. The 'Gene Study' functionality of CFX Manager was utilised. For (i) $n=3$ for ARPE-19A cells and $n=6$ for ARPE-19B cells; for (ii) $n=3$ for podocytes. See supplementary material Table S2 for details of *n*-values for ARPE-19A and ARPE-19B cells. (B) Immunofluorescence microscopy of ARPE-19A and ARPE-19B cells, and podocytes (all 7 days), showing localisation of ZO-1 (black and white, green), with nuclei stained with DAPI (blue). Localisation of tight junction protein ZO-1 at cell–cell junctions was detected only in ARPE-19A cells (arrows). Images were taken using a 60× objective. Scale bars: 25 μm. Representative images from $n=2$ experiments are shown. (C) Cell lysates of ARPE-19A and ARPE-19B cells were separated on 4–12% Bis-Tris gels in reducing conditions, and analyzed by western blotting for E-cadherin or β-actin. E-cadherin was detected only in ARPE-19A cultures. β-actin was loading control. (D) Immunofluorescence microscopy of ARPE-19A and ARPE-19B cells, and podocytes (7 days), showing localisation of N-cadherin, E-cadherin and β-catenin (green), with nuclei stained with DAPI (blue). Images were taken using a 60× objective. Scale bars: 25 μm. Representative images from $n=2$ experiments are shown.

Journal of Cell Science (2014) 127, 158–171 doi:10.1242/jcs.134270

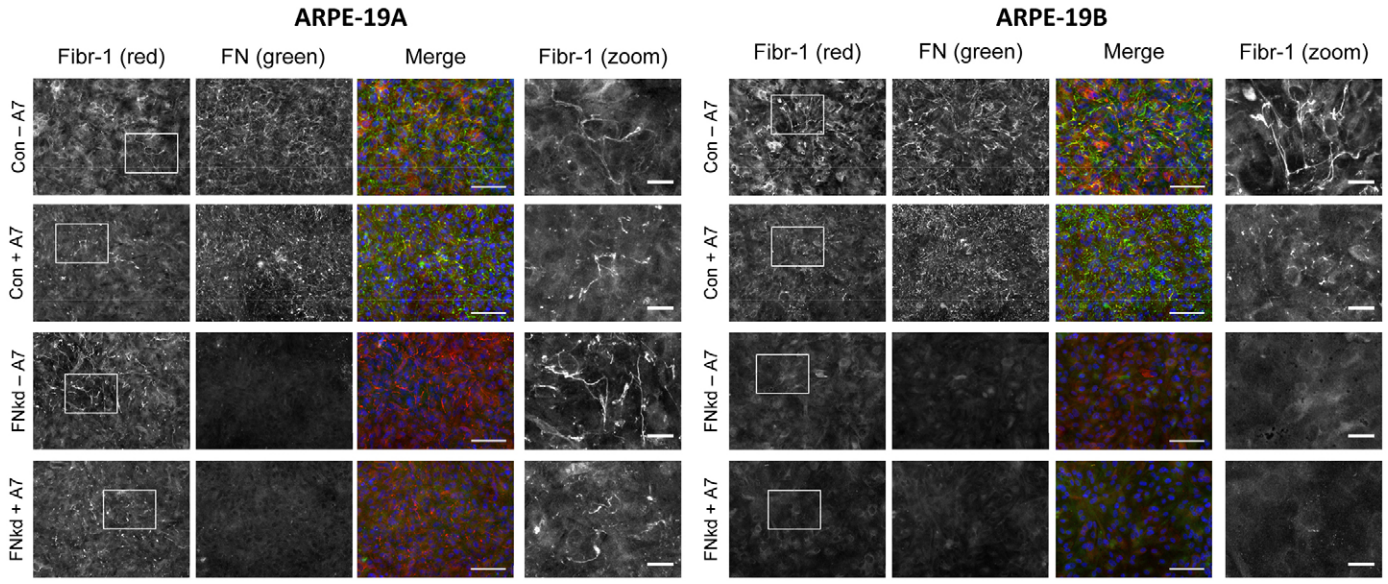

Fig. 3. Effects of cadherin-blocking peptide on microfibril and FN deposition by ARPE-19A and ARPE-19B cultures. Immunofluorescence microscopy of ARPE-19A and ARPE-19B (control and FN kd, 7 days), showing deposition of fibrillin-1 (Fibr-1; black and white, red) and FN (black and white, green), with nuclei stained with DAPI (blue), in the presence or absence of the cadherin-blocking peptide A7 (Devemy and Blaschuk, 2009). Images were taken using a 20× objective. Specific band-pass filter sets for DAPI, FITC and Cy3 or Cy5 were used to prevent bleed-through. Boxed areas are shown as zoomed images on right. Scale bars: 100 μm (for first three lanes); 25 μm (zoom).

Syndecan involvement in microfibril deposition

Syndecans interact with FN and integrin receptors (Couchman, 2010). qPCR analysis of the relative abundance of syndecan receptors 1–4 revealed that, in all cultures, syndecan-2 and -4 were most abundant (supplementary material Fig. S2A). Podocytes had highest levels of syndecan-1 and -4, and lowest levels of syndecan-2. All ARPE-19 cultures had low levels of syndecan-1. FN knockdown had little effect on syndecan expression (supplementary material Fig. S6C). Fluorescence-activated cell sorting (FACS) confirmed that podocytes expressed the highest levels of syndecan-4, and that it was depleted upon knockdown (Fig. 4D). Hence, we tested whether either syndecan was required for microfibril deposition by ARPE-19 cells or podocytes (Fig. 4; supplementary material Fig. S5D).

Syndecan-2 is not required for microfibril deposition

Knockdown of syndecan-2 with siRNA treatment that was repeated every 48 hours resulted in syndecan-2 knockdown by 97% compared to lipofectamine-treated control ARPE-19A cells, by 99% in ARPE-19B cells, and 97% in HDFs (supplementary material Fig. S3E–G). Western blotting of the syndecan-2 knockdown cells showed abundant FN and fibrillin-1 in medium and cell layer extracts (Fig. 1D; supplementary material Fig. S1C). After syndecan-2 depletion, microfibrils were deposited by all cultures, especially ARPE-19A (Fig. 4; supplementary material Fig. S5D). Hence, overall, syndecan-2 is not essential for microfibril deposition.

Syndecan-4 is required for microfibril deposition by ARPE-19A and podocytes

Syndecan-4 was knocked down every 48 hours for 7 days in ARPE-19A cells (96% knockdown), ARPE-19B cells (96% knockdown) and in podocytes (98% knockdown), or for 8 days in HDFs (95% knockdown) (supplementary material Fig. S3E–G; Fig. S6A). Western blotting of revealed that, compared to lipofectamine-treated ARPE-19 cultures, ARPE-19A syndecan-4 knockdown cultures had grossly reduced fibrillin-1 levels in medium (Fig. 1D). ARPE-19B syndecan-4 knockdown cultures had reduced fibrillin-1, and FN, in medium. Podocytes secreted fibrillin-1 into medium that appeared unprocessed, as judged by slower migration (Fig. 1E). Immunofluorescence microscopy showed that ARPE-19A and podocytes, but not ARPE-19B cultures (Fig. 4), required syndecan-4 for microfibril deposition. Syndecan-4 localised at podocyte cell–cell junctions (Fig. 6A). Syndecan-4 knockdown HDF cultures had reduced microfibrils (supplementary material Fig. S5D).

As syndecan-4 can internalise α5β1 integrin in fibroblasts (Bass et al., 2011; Morgan et al., 2013), we investigated the presence of surface β1 integrin (antibody MAR4) following syndecan-4 siRNA treatment in ARPE-19 cultures. Flow cytometry, at 24 hours post-knockdown, revealed no changes in β1 integrin levels, and microscopy did not detect changes in actin organisation (not shown).

ARPE-19 cells vary in dependency on PKCα for microfibril deposition

Syndecan-4 binds to, and can stimulate, PKCα, which in turn regulates Rho GTPases (Couchman, 2010). We investigated whether PKCα underpins dependency on syndecan-4 for microfibril deposition by ARPE-19A cells (Fig. 4; supplementary material Fig. S5D).

We treated cells with siRNA targeting PKCα every 48 hours (85% PKCα knockdown in ARPE-19A cells at 7 days, 74% PKCα knockdown in ARPE-19B cells at 7 days, and 92% PKCα knockdown in HDFs at 8 days) (supplementary material Fig. S3E–G). In ARPE-19A cultures, PKCα depletion significantly reduced mRNA levels of fibrillin-1 and FN (supplementary material Fig. S3E). Western blotting confirmed reduced PKCα protein in ARPE-19 cells (supplementary material Fig. S3H). Blotting revealed that PKCα knockdown in ARPE-19B cells markedly reduced fibrillin-1, and also FN, in cell layer extracts

Journal of Cell Science (2014) 127, 158–171 doi:10.1242/jcs.134270

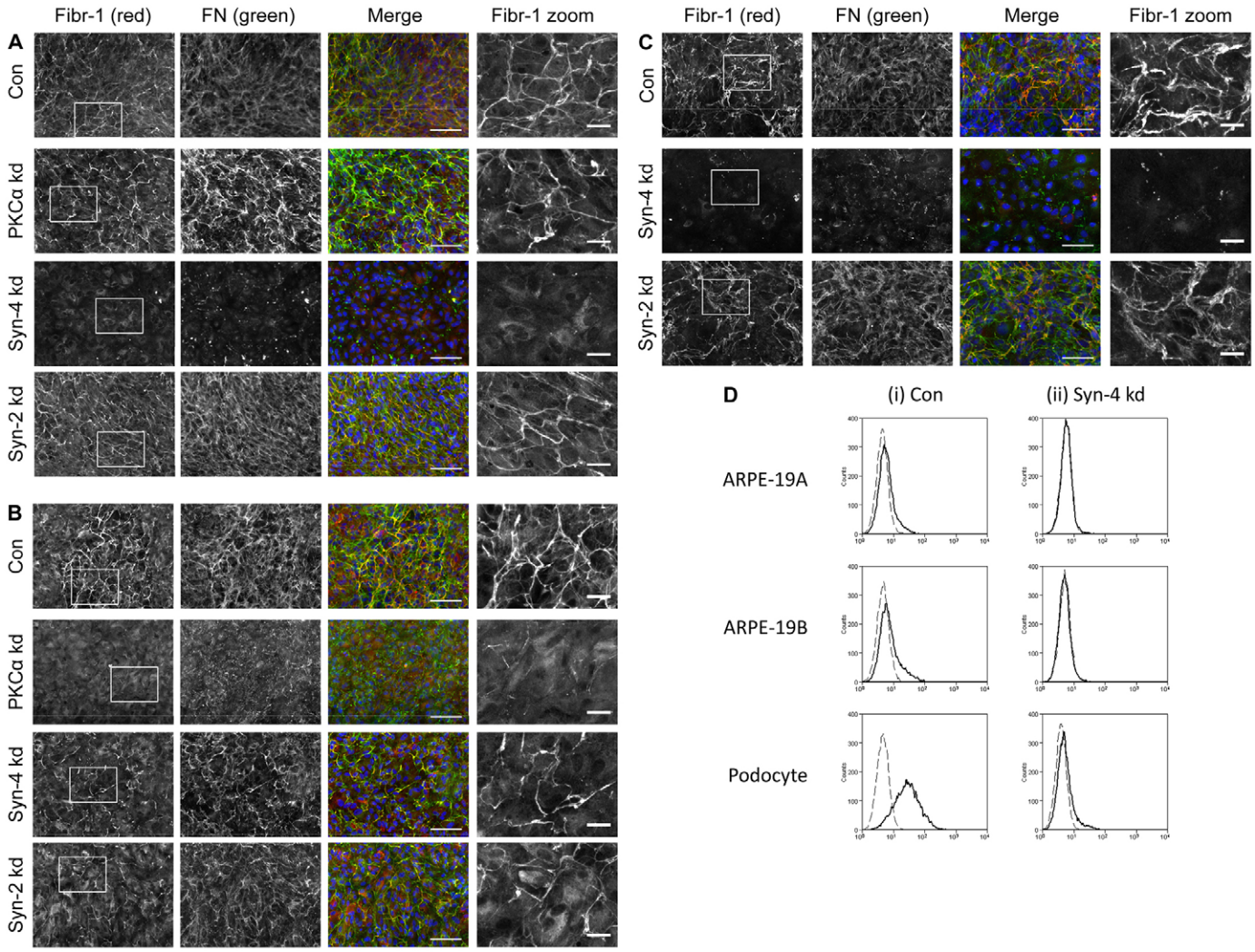

Fig. 4. Effects of depleting syndecan-2 or syndecan-4, or PKCα, on microfibril deposition by ARPE-19 cells and podocytes. Immunofluorescence microscopy of (A) ARPE-19A cells, (B) ARPE-19B cells and (C) podocytes (all after 7 days), showing deposition of fibrillin-1 (Fibr-1; black and white, red) and FN (black and white, green), with nuclei stained with DAPI (blue). Images were taken using a 20× objective. Specific band-pass filter sets for DAPI, FITC and Cy3 or Cy5 were used to prevent bleed-through. Boxed areas are shown as zoomed images on right. ARPE-19A and ARPE-19B control cultures (Con) showed partial colocalisation of fibrillin-1 and FN (yellow). Syndecan-4 knockdown (kd) ARPE-19A cells had no microfibrils or FN fibrils. In contrast, syndecan-4 kd ARPE-19B cells had prominent microfibrils and FN. PKCα kd ARPE-19A cells had prominent microfibrils and FN, whereas PKCα ARPE-19B cultures had no microfibrils and few FN fibrils. Syndecan-2 kd did not block FN deposition and microfibril formation in either ARPE-19A or B cells. Syndecan-4 kd podocytes had no microfibrils or FN fibrils, but knockdown of syndecan-2 did not disrupt FN deposition and microfibril formation. Scale bars: 100 μm (for first three lanes); 25 μm (zoom). Representative images from $n=4$ (A,B) and $n=3$ (C) experiments are shown. (D) Flow cytometry traces showing levels of syndecan-4 at cell surfaces of ARPE-19A and ARPE-19B cells, and podocytes, in control and syndecan-4 knockdown cells. Labelling with anti-syndecan-4 antibody 5g9 (solid lines) revealed low levels of syndecan-4 at the cell surface of ARPE-19A and ARPE-19B cells, compared to secondary antibody-only controls (dashed lines). Podocyte cultures had higher levels of syndecan-4 than ARPE-19 cultures. siRNA knockdown of syndecan-4 was effective in all cultures.

(Fig. 1D). Immunofluorescence microscopy revealed that, following PKCα knockdown, microfibrils were detected in ARPE-19A cultures, but not ARPE-19B cultures or HDFs (Fig. 4; supplementary material Fig. S5D).

Thus, dependency of epithelioid ARPE-19A cells on syndecan-4 for microfibril deposition does not involve PKCα; however, mesenchymal ARPE-19B cells and HDFs require PKCα.

ARPE-19 cells require α5β1 and/or α8β1 integrins for microfibril deposition

We have previously shown that disrupting FN RGD or α5β1 integrin inhibits microfibril deposition in fibroblasts (Kinsey et al., 2008). As fibrillin-1 can bind α5β1 and αvβ3, and αvβ6 in keratinocytes (Bax et al., 2003; Jovanovic et al., 2007), and perlecan can bind α2β1 (Bix et al., 2004) and α8β1 (Sato et al., 2013), and as epithelial cells express these integrins, we explored their involvement in microfibril deposition by ARPE-19 cultures (Fig. 5).

Incubation of ARPE-19A cells with function-blocking antibodies to α2β1 (Gi9; also JA218, not shown), α5 (mAb16), α8 (T-20), β1 (mAb13), αv (17E6), αvβ3 (LM609 and 23C6; not shown) or αvβ6 (10D5) integrins revealed that microfibril deposition was blocked by antibodies to α8 and β1, reduced by antibodies to α5, but not by antibodies to αv, αvβ6, αvβ3 or α2β1 (Fig. 5A; αvβ3 not shown). When ARPE-19B cultures were treated with the same integrin-blocking antibodies, microfibril

Journal of Cell Science (2014) 127, 158–171 doi:10.1242/jcs.134270

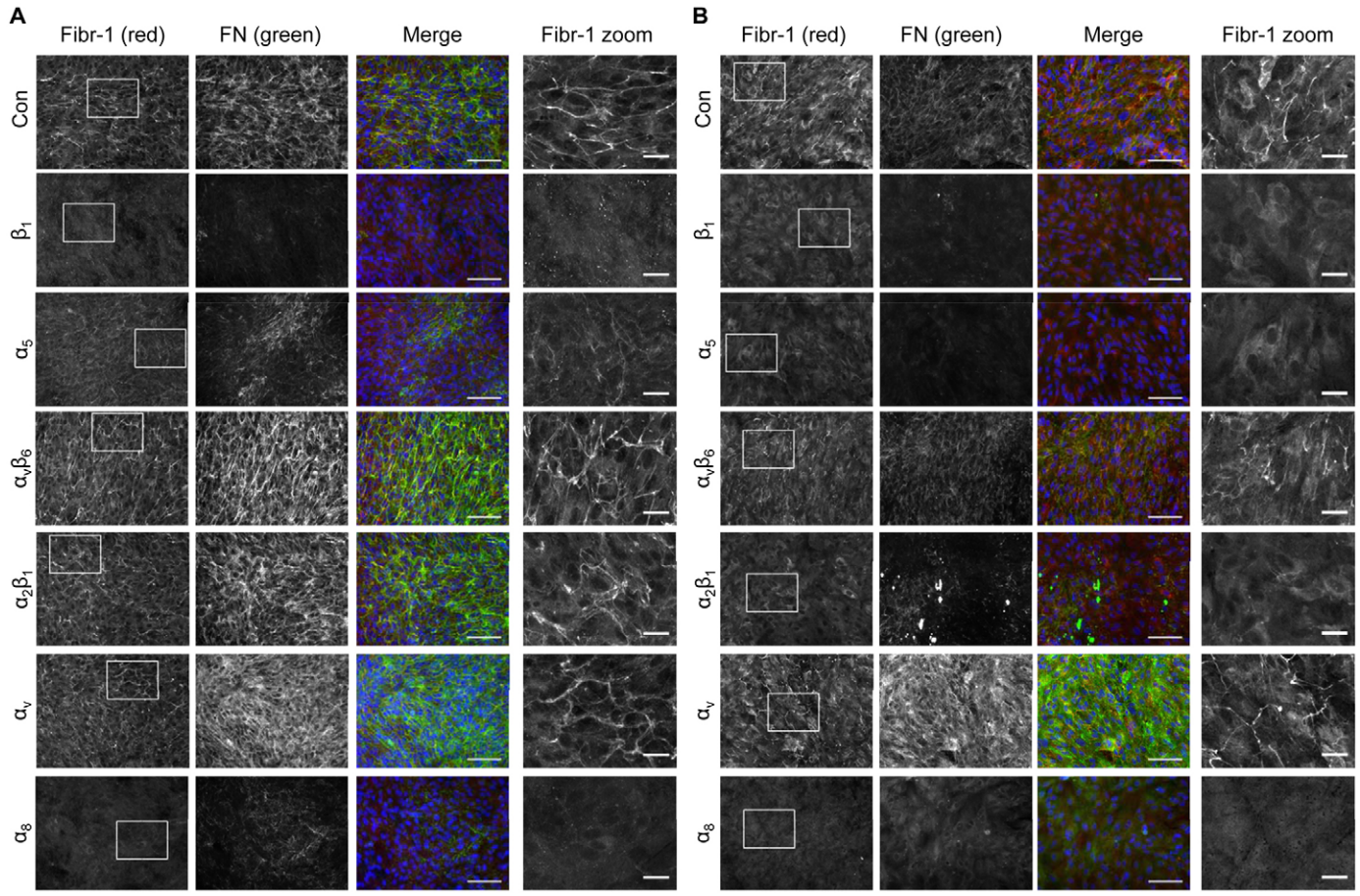

Fig. 5. Effects of integrin blocking on microfibril and FN deposition by ARPE-19A and ARPE-19B cultures. Immunofluorescence microscopy of fibrillin-1 (Fibr-1) and FN in (A) ARPE-19A cultures and (B) ARPE-19B cultures after 7 days in the presence of integrin function-blocking monoclonal antibodies (mAb), as indicated, or no mAb (Con), or non-functional mAb11 (not shown), highlighting deposition of fibrillin-1 (black and white, red) and FN (black and white, green), with nuclei stained with DAPI (blue). Images were taken using a 20× objective. Specific band-pass filter sets for DAPI, FITC and Cy3 or Cy5 prevented bleed-through. Boxed areas are shown as zoomed images on right. (A) ARPE-19A control cultures had microfibrils and FN; cultures treated with blocking mAbs to αvβ6 (10D5), α2β1 (Gi9; also JA218, not shown) showed robust microfibrils and FN; cultures treated with anti-αv (17E6) had microfibrils and prominent cell-associated FN; cultures treated with anti-α5 (mAb16) had greatly reduced microfibrils and FN; microfibrils were not detected in cultures treated with anti-α8 (T-20) but did have traces of FN; microfibrils and FN were not detected in cultures treated with anti-β1 (mAb13). Scale bars: 100 μm (for first three lanes); 25 μm (zoom). (B) ARPE-19B control cultures had microfibrils and FN; cultures treated with anti-αvβ6 (10D5), showed robust microfibrils and FN; cultures treated with anti-αv (17E6) had microfibrils and prominent cell-associated FN; microfibrils were not detected in cultures treated with anti-α2β1 (Gi9), anti-α8 (T-20) and anti-α5 (mAb16) but did have traces of FN; cultures treated with anti-β1 (mAb13) had no detectable microfibrils or FN. Scale bars: 100 μm (for first three lanes); 25 μm (zoom). Representative images from $n=2$ experiments are shown.

deposition was blocked by inhibition of α5β1 or α8β1 integrins, and by α2β1, but not by αv integrins (Fig. 5B). Thus, both cultures require α8β1 integrin, ARPE-19A cells show partial dependency on α5β1, and ARPE-19B cells require α2β1. Neither culture needed αv integrins for microfibril deposition.

ARPE-19 cells required HS biosynthesis for microfibril deposition

HS is a component of syndecan receptors that binds FN (Couchman, 2010), and it strongly interacts with fibrillin-1 (Cain et al., 2008; Tiedemann et al., 2001). Immunofluorescence localisation of HS in the ARPE-19 cultures revealed that HS (antibody 10E4) was concentrated at ARPE-19A cell–cell junctions and showed little colocalisation with FN (antibody FN-3E2) (not shown). Podocytes had abundant HS staining, which appeared partially extracellular.

To explore whether HS influences the differential deposition of microfibrils by ARPE-19A and ARPE-19B cells (Figs 1, 4), we knocked down exostosin-1 (EXT1), an early enzyme in the HS synthetic pathway. EXT1 depletion inhibits HS biosynthesis, with only short sulfated chains generated (Busse et al., 2007; Osterholm et al., 2009), and impairs focal adhesions (Mahalingam et al., 2007). EXT1 siRNA was repeated every 48 hours (supplementary material Fig. S3A–C). Immunostaining for HS confirmed greatly reduced HS in all cases (not shown). Immunofluorescence microscopy revealed that FN was deposited pericellularly as short arrays, but fibrillin-1 appeared intracellular (Fig. 6B; supplementary material Fig. S7B). EXT1 knockdown increased expression of fibrillin-1 by ARPE-19 cells and HDFs, as judged by qPCR; ARPE-19A cells had reduced FN (supplementary material Fig. S3A–C). Western blots of ARPE-19A and ARPE-19B medium after EXT1 knockdown showed reduced fibrillin-1 compared to control cells (Fig. 1D), but in cell layer extracts, there was increased fibrillin-1 compared to control cells. EXT1 knockdown in HDFs did not alter fibrillin-1 levels in cell layer extracts (supplementary material Fig. S1B). In ARPE-19A and ARPE-19B cells, there was also significantly enhanced

Journal of Cell Science (2014) 127, 158–171 doi:10.1242/jcs.134270

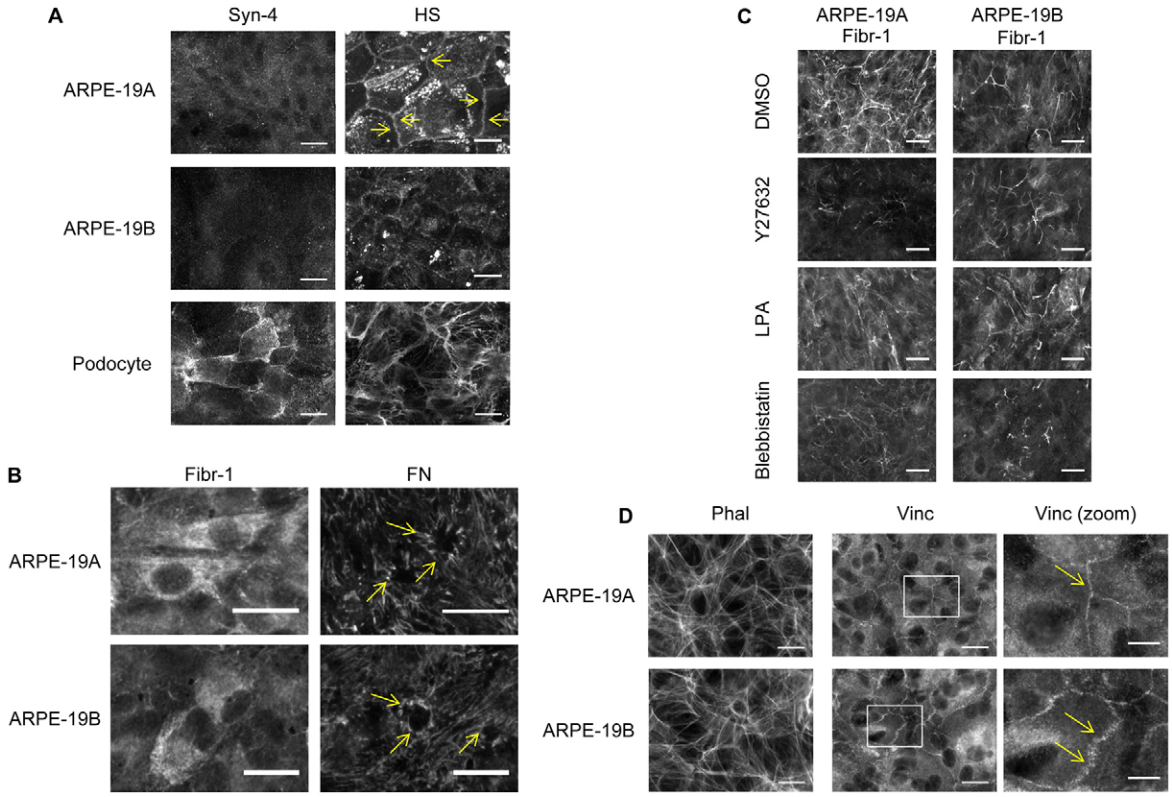

Fig. 6. Effects of actomyosin inhibitors or HS depletion on ARPE-19 cultures. (A) Immunofluorescence microscopy of ARPE-19 cells and podocytes (after 7 days), showing localisation of syndecan-4 and HS. For ARPE-19A cells in particular, HS localised at cell–cell contacts (arrows). Images were taken using a 20× objective. Scale bars: 25 μm. Representative images from $n=2$ experiments are shown. (B) Immunofluorescence microscopy of ARPE-19A and ARPE-19B cells (cultured for 7 days) following knockdown of EXT1 (depleting HS). Images were taken using a 20× objective. EXT1 knockdown in both ARPE-19 cultures ablated microfibrils, with only cellular fibrillin-1 staining and punctate pericellular FN (arrows). Scale bars: 25 μm. Representative images from $n=4$ experiments are shown. For microscopy, specific band-pass filter sets for DAPI, FITC, and Cy3 or Cy5 were used to prevent bleed-through. (C) Immunofluorescence microscopy of ARPE-19 cells (cultured for 7 days), showing deposition of fibrillin-1 (Fibr-1). Images were taken using a 20× objective. Cells were incubated for 7 days in the presence of myosin II inhibitor blebbistatin (10 μM), or Rho kinase inhibitor Y27632 (10 μM), or RhoA activator lysophosphatidic acid (LPA) (20 μM), with DMSO controls (DMSO). Microfibrils were reduced in all cells treated with blebbistatin or Y27632. Scale bars: 25 μm. Representative images from $n=2$ experiments are shown. (D) Immunofluorescence microscopy of ARPE-19 cells (cultured for 7 days), showing localisation of phalloidin (Phal) and vinculin (Vinc). Vinculin accumulated at cell-cell contacts in ARPE-19A and ARPE-19B cells; in ARPE-19B cells, these junctions appeared under tension. Phalloidin staining was similar in ARPE-19A and ARPE-19B cells. Images were taken using a 60×objective. Boxed areas are shown as zoomed images on right. Scale bars: 25 μm (for first two lanes); 10 μm (zoom). Representative images from $n=2$ experiments are shown.

E-cadherin expression (supplementary material Fig. S6B). In HDF cultures, EXT1 knockdown induced disordered microfibrils, but FN fibrils appeared unaffected (supplementary material Fig. S1A).

Thus, HS biosynthesis regulates microfibril assembly. Although EXT1 siRNA in ARPE-19 cells enhanced fibrillin-1 expression, it also disrupted its secretion and assembly. As fibrillin-1 deposition by both ARPE-19 cultures was similarly affected by EXT1 siRNA, HS cannot underlie their differential FN dependency for microfibril deposition.

ARPE-19 cells require cytoskeletal tension for microfibril deposition

We next investigated whether contractile cytoskeleton is necessary for microfibril deposition by ARPE-19 cells, using cytoskeletal inhibitors every 48 hours over 7 days (Fig. 6C; supplementary material Fig. S7). In both ARPE-19 cultures, blebbistatin inhibition of myosin II or Y-27632 inhibition of Rho kinase inhibited FN and microfibril deposition. The RhoA activator lysophosphatidic acid did not further enhance microfibril deposition. Vinculin links integrins and cell junctions to actin (Braga et al., 1997; Terry et al., 2011; Yamada and Nelson, 2007); both cultures had prominent pericellular vinculin, with many ARPE-19B cell junctions under tension (Fig. 6D). Thus, contractile actomyosin was needed for microfibril deposition by ARPE-19 cells.

Effects of TGFβ on ARPE-19A and ARPE-19B cells, and podocytes

As TGFβ can induce EMT (Kalluri and Weinberg, 2009), we investigated how TGFβ affects microfibril deposition by ARPE-19 cells and podocytes (Fig. 7).

For ARPE-19A control cells, TGFβ increased fibrillin-1 expression 3-fold, and thick microfibrils were deposited. In FN siRNA cells, TGFβ increased fibrillin-1 expression >3-fold; microfibrils were deposited with or without TGFβ. In syndecan-4 siRNA cells, TGFβ increased fibrillin-1 expression 1.8-fold; some colocalising microfibrils and FN were present. ARPE-19A cells had ZO-1-staining junctions with or without TGFβ (Fig. 2B; not shown).

For ARPE-19B control cells, TGFβ increased fibrillin-1 expression ~3-fold, and microfibrils were deposited. In FN siRNA cells, TGFβ increased fibrillin-1 expression >2-fold, but there were no microfibrils. In syndecan-4 siRNA cells, TGFβ

Journal of Cell Science (2014) 127, 158–171 doi:10.1242/jcs.134270

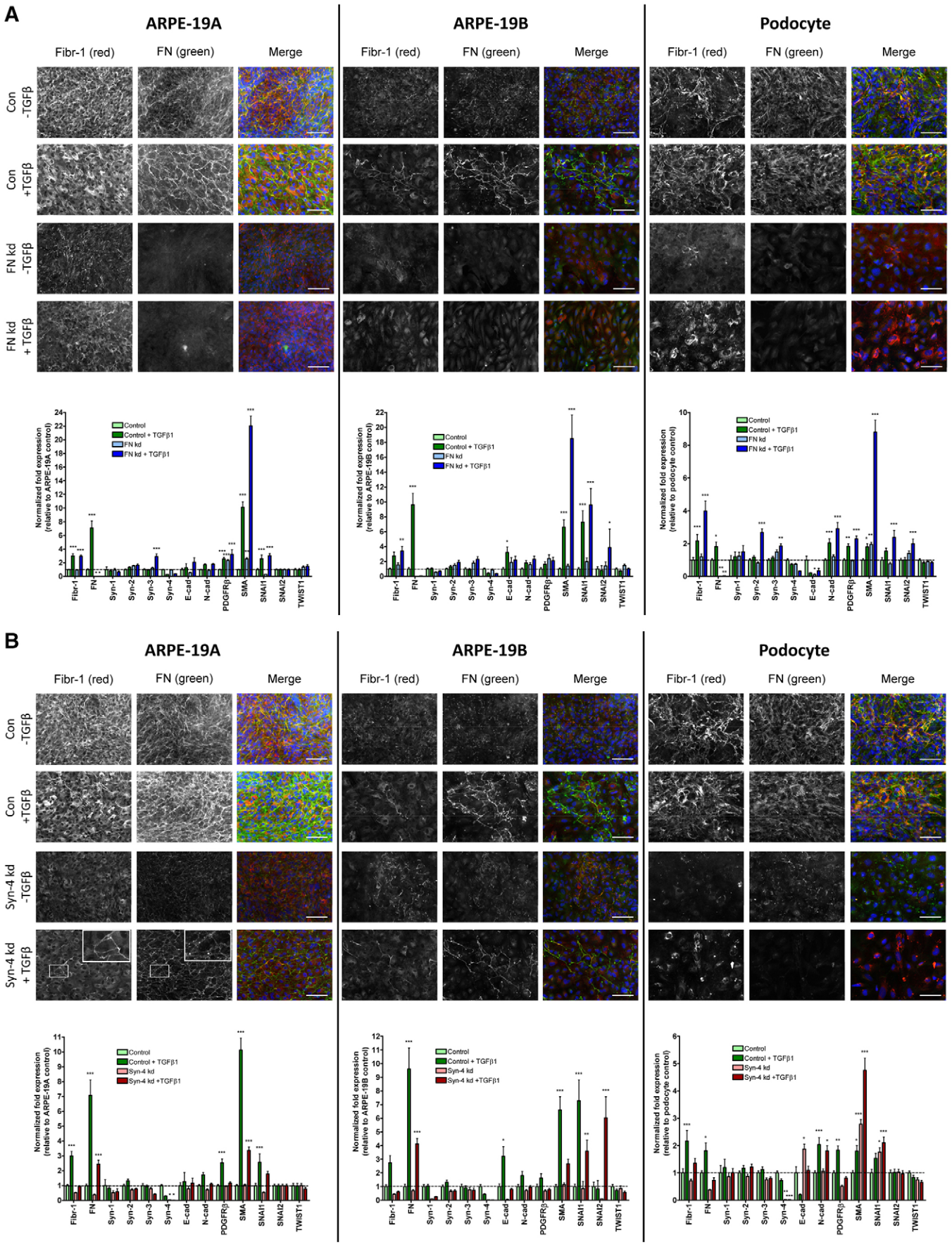

Fig. 7. See next page for legend.

Journal of Cell Science (2014) 127, 158–171 doi:10.1242/jcs.134270

Fig. 7. Effects of TGFβ1 on microfibril deposition by ARPE-19 cells and podocytes. Immunofluorescence microscopy of deposition of fibrillin-1 (Fibr-1; black and white, red) and FN (black and white, green) was conducted, along with real-time quantitative PCR (qPCR) analysis of gene expression in ARPE-19A and ARPE-19B cells, and podocytes (all 7 days) which were cultured in the presence or absence of 160 pM TGFβ1. TGFβ1 was added to control cultures, and to (A) FN knockdown (kd) and (B) syndecan-4 kd cultures. Gene expression of fibrillin-1 (Fibr-1), fibronectin (FN), syndecans (syn) 1–4, E-cadherin (E-cad), N-cadherin (N-cad), PDGF receptor-β (PDGFRβ), smooth muscle α-actin (SMA), SNAI1, SNAI2 and TWIST 1 is shown. Expression was normalised using a combination of GAPDH and TATA box binding protein (TBP) expression, and reported relative to expression levels in ARPE-19A control cultures with no added TGFβ1 (where ARPE-19A control expression was set at 1). All data are represented as mean±s.e.m. and were analyzed by two-way ANOVA. $^{*}P<0.05$; $^{**}P<0.01$; $^{***}P<0.001$. The 'Gene Study' functionality of CFX Manager was utilised. For microscopy, nuclei were stained with DAPI (blue); Scale bars: 100 μm. $n=2$ for all samples. Boxed area is shown as a zoom in the top right-hand corner for ARPE-19A syn-4 kd cells with TGFβ1.

increased fibrillin-1 expression 1.4-fold; microfibrils and FN were seen. ARPE-19B cells had no ZO-1-staining junctions with or without TGFβ (Fig. 2B; not shown).

For control podocytes, TGFβ increased fibrillin-1 expression >2-fold, and microfibrils were abundant. In FN siRNA cells, TGFβ increased fibrillin-1 expression >3-fold; some microfibrils were seen. In syndecan-4 siRNA cells, TGFβ increased fibrillin-1 expression ~2-fold; staining was pericellular. No ZO-1-staining junctions were seen with or without TGFβ (Fig. 2B; not shown).

TGFβ1 had many other effects on gene expression; in particular it enhanced expression of FN, PDGFRβ and SMA in all cells, and SNAI2 in FN-depleted ARPE-19B cells (Fig. 7). Following FN siRNA, TGFβ did not alter cell-specific dependencies on FN. TGFβ did induce deposition of fibrillin-1 and FN in syndecan-4 siRNA ARPE-19A cells, which colocalised, thus overcoming dependency on syndecan-4 for microfibril deposition in these cells.

In summary, we have shown epithelial–mesenchymal cell-specific mechanistic differences in ECM deposition.

DISCUSSION

The discovery that mesenchymal cells require FN to deposit fibrillin microfibrils (Kinsey et al., 2008; Sabatier et al., 2009) was unexpected from an evolutionary perspective (Ozbek et al., 2010). We have explored this relationship by comparing HDFs with ARPE-19 cells (Cain et al., 2009; Massam-Wu et al., 2010) and podocytes (Lennon et al., 2013), all of which deposit ECM. Our data show that FN is not essential for microfibril formation by all cells, and we identify roles for syndecan-4, HS and epithelial cell–cell junctions in microfibril deposition.

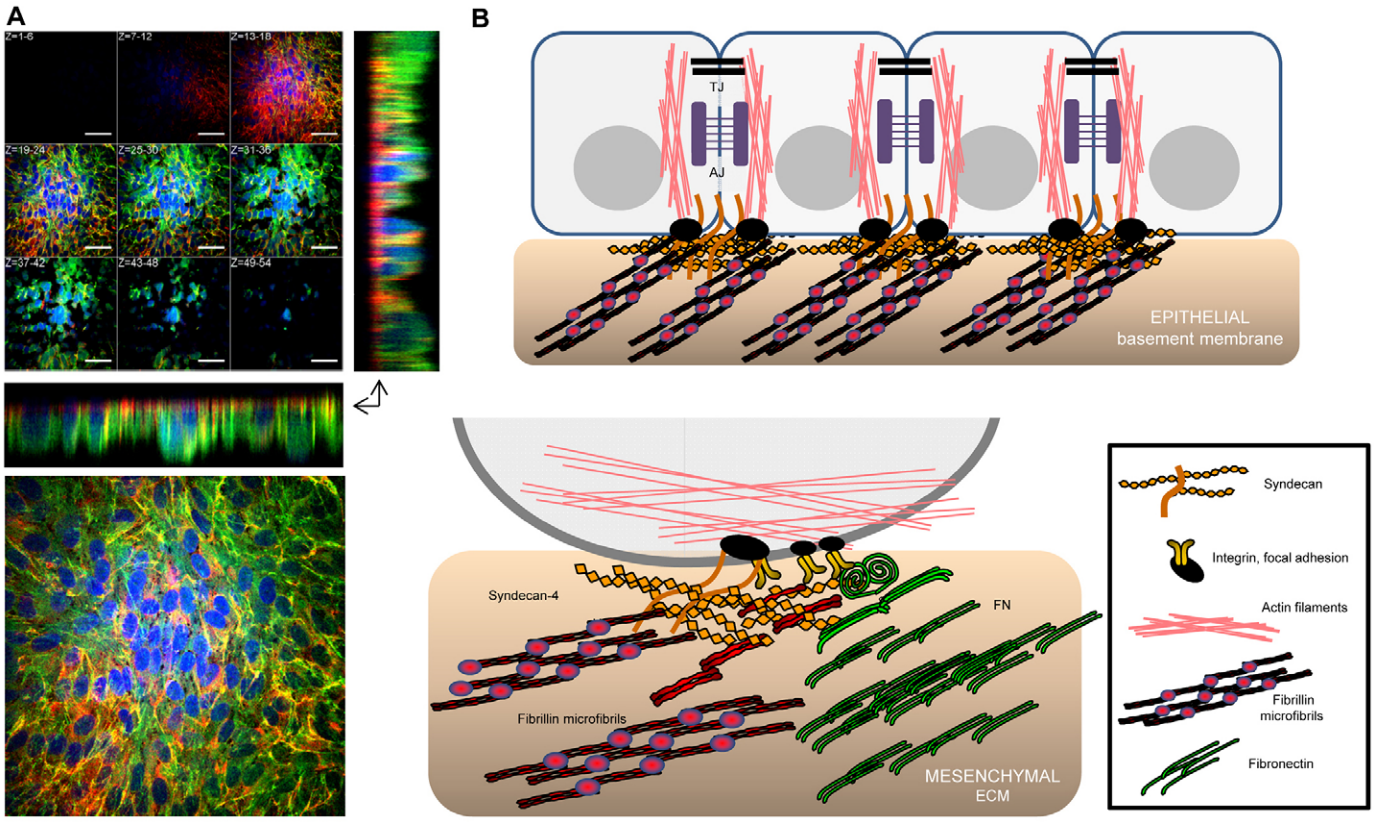

Fig. 8. Pericellular microfibril assembly. (A) Confocal microscope image of ARPE-19A cells (after 7 days) showing deposition of fibrillin-1 (red) and FN (green). The montage shows a *z*-stack of 54 images grouped in sets of six slices. The focus starts at the surface of the glass coverslip and moves to the top of the cell. Fibrillin-1 microfibrils are deposited on the surface of the coverslip and the FN fibrils above fibrillin-1. Also shown is the *xz* and *yz* projections of the original image stack. Scale bars: 50 μm. Images were taken with a 60× objective on a Nikon C1 upright confocal. (B) Model of how epithelial–mesenchymal status might influence microfibril assembly, with newly secreted fibrillin-1 aligned for assembly by HS-rich focal adhesions that are differentially induced by epithelial cell–cell junctions or mesenchymal FN.

Journal of Cell Science (2014) 127, 158–171 doi:10.1242/jcs.134270

We found that epithelial ARPE-19A cells are not dependent on FN or PKCα for microfibril deposition, unlike the more-mesenchymal ARPE-19 cells. Deposition of perlecan, an unrelated ECM molecule, has similar cell-specific dependencies to that of FN, which are thus not unique to fibrillin-1. Although podocytes (which have specialised slit-diaphragm junctions with components of tight and adherens junctions) can also assemble microfibrils after FN depletion, abundant microfibril deposition required FN, indicating that FN is required for this process to be efficient.

We found that HS biosynthesis was also required for fibrillin-1 secretion and microfibril deposition by ARPE-19 cells. Heparin/HS strongly binds fibrillin-1 (Cain et al., 2008; Tiedemann et al., 2001) and might be needed to direct assembly interactions. As FN formed only short pericellular arrays after HS knockdown, HS also influences FN fibrillogenesis, yet the extracellular presence of FN but not microfibrils in these experiments argues against FN as a template for fibrillin-1. Furthermore, microfibrils were disrupted by HS depletion in HDF cultures, which had abundant FN. In FN-dependent ARPE-19B cells, deletions of EXT1 or PKCα also depleted extracellular FN, which might have contributed to their reduced microfibrils.

How then might FN enhance microfibril deposition in a cell-specific manner? Given the need for HS, its localisation at cell–cell junctions in epithelioid ARPE-19A cultures implies that it has a role in FN-independent microfibril assembly. Another clue might lie in our discovery of the essential role for α8β1 integrin in microfibril assembly by ARPE-19 cells; the requirement for α5β1 and/or α8β1 integrins, and cytoskeletal tension for microfibril deposition by ARPE-19 cells confirms our earlier HDF data (Kinsey et al., 2008). α8β1, like α5β1, can engage FN but it also binds nephronectin, which is needed for epithelial–mesenchymal interactions in kidney development (Hartner et al., 2012; Müller et al., 1997; Sato et al., 2013). Thus, the cell-specific balance of activating (or inhibiting, e.g. fibulin-5; Lomas et al., 2007) ligands for α5β1 or α8β1 integrins might regulate cytoskeletal tension and focal adhesion formation.

The contributions of syndecans to microfibril assembly were complex. Whereas syndecan-2 was not essential for microfibrils, syndecan-4, but not its effector PKCα, was needed by ARPE-19A cells and podocytes for fibrillin-1 secretion and assembly. Given that syndecan-4 is a component of focal adhesions (Gopal et al., 2010; Woods et al., 2000), it could be needed to form cytoskeletally linked adhesions at cell junctions. Syndecan-1, which is implicated in EMT, could serve a similar role in other epithelial cells (Masola et al., 2012; Stepp et al., 2007).

It is unclear why cFN did not effectively rescue microfibrils in ARPE-19B cells or why podocytes needed FN for efficient microfibril deposition. A general possibility is that their cell–cell organisation was insufficient to support assembly. Because only ARPE-19A cells had defined HS-rich tight junctions, tight junctions could be necessary for the FN-independent microfibril deposition in these cells. The more-mesenchymal cells that lack tight junctions might instead rely on FN to induce HS-rich focal adhesions. ARPE-19A cells and podocytes also have adherens junctions, which affect microfibril deposition, as they function in the FN assembly by certain epithelial cells (Dzamba et al., 2009). Given that blocking cadherin interactions induced short FN arrays resembling those after HS depletion, FN assembly might also require HS-rich cell junctions.

EMT involves complex cellular changes (Thiery and Sleeman, 2006; Kalluri and Weinberg, 2009), and can be induced by TGFβ, which upregulates FN and SMA (Fig. 7). Marker analysis suggested that cultured ARPE-19 cells were in epithelioid or mesenchymal states and that podocytes were in transition. TGFβ1 partially overcame the dependency on syndecan-4 for fibrillogenesis in epithelioid ARPE-19A cells, inducing colocalised microfibrils and FN, which implies induction of FN dependency. The reason for differences between batches of ARPE-19 cultures is unclear, but some clonal sublines are known to be more fibroblast-like (Dunn et al., 1996) and they are sensitive to EMT (Chen et al., 2012; Huang et al., 2013; Li et al., 2011; Tamiya et al., 2010; Tian et al., 2005).

We propose a microfibril assembly model (Fig. 8) that is compatible with pre-chordates, which lack FN (Esko and Lindahl, 2001; Hynes, 2012; Johnson et al., 2009; Ozbek et al., 2010; Tucker and Chiquet-Ehrismann, 2009). In epithelioid cells with cell–cell junctions, microfibrils assemble pericellularly and basally (Fig. 8A), enabled by junction-induced (FN-independent) focal adhesions comprising HS and/or syndecan, and β1 integrin, linked to cortical cytoskeleton (Braga et al., 1997; Nakajima and Tanoue, 2011; Smith et al., 2012; Terry et al., 2011; Yamada and Nelson, 2007). In mesenchymal cells, FN induces mobile syndecan-rich focal assembly sites.

In summary, we have shown that ECM deposition is regulated by epithelial–mesenchymal status. Dependency on FN might be an evolutionary acquisition to support the deposition of robust fibrillar mesenchymal tissues.

MATERIALS AND METHODS

Cell culture

HDFs were purchased from Life Technologies (UK). Three batches of ARPE-19 cells were independently purchased from the American Tissue Culture Collection (CRL-2302). Cells designated ARPE-19A were batch 58280268, cells designated ARPE-19B were batch 59270158, and cells designated ARPE-19C were batch 60279299. These cells were maintained in Dulbecco's modified Eagle's medium (DMEM; Sigma-Aldrich) supplemented with 10% (v/v) fetal calf serum (FCS; Life Technologies), 1% L-glutamine, 100 U/ml penicillin-streptomycin at 37℃ in 5% CO_2, and were routinely passaged at confluency.

Conditionally immortalised human podocytes (Saleem at al., 2002) were grown on uncoated tissue culture plates. Podocytes between passage 24 and 30 were cultured for 7 days at 33℃ in RPMI-1640 medium with glutamine (R-8758; Sigma, St. Louis, MO, USA) supplemented with 10% (v/v) FCS (Life Technologies), 5% (v/v) ITS (I-1184; Sigma; 1 ml/100 ml) and 100 U/ml penicillin-streptomycin. In these conditions, podocytes are proliferating and have a 'cobblestone' (epithelial) phenotype. HaCaT cells were grown in DMEM (Sigma-Aldrich), supplemented with 10% (v/v) FCS (Life Technologies), 1% L-glutamine, 100 U/ml penicillin-streptomycin, at 37℃ in 5% CO_2, and were passaged at confluency. Mammary epithelial cells (MCF10A) were cultured as described (Debnath et el., 2003).

Cell lines ARPE-19A and ARPE-19B were confirmed to be ARPE-19 cells, and the identity of mammary epithelial cells MCF10A was also confirmed using the Promega Powerplex 16 HS system. STR (short tandem repeats) analysis was carried out using an Applied Biosystems 3730 DNA Analyzer using Applied Biosystems POP-7 polymer. STR data for HaCaT and podocytes were not available.

Antibodies

Primary antibodies for immunofluorescence microscopy were against FN (FN-3E2, Sigma-Aldrich; 1:200), fibrillin-1 (HPA021057, Sigma-Aldrich, 1:200; mAb 11C1.3, Abcam, 1:200), HS (10E4, Seigagaku, Japan; 1:200), perlecan (A7L6, Millipore; 1:200), β1 integrin (B44, Millipore; 1:200) and ZO-1 (T11, Millipore; 1:200). Anti-vinculin antibody (hVin-1, Sigma-Aldrich; 1:400) was used to identify focal adhesions, and phalloidin conjugated to Rhodamine (Life Technologies;

Journal of Cell Science (2014) 127, 158–171 doi:10.1242/jcs.134270

1:1000) to stain the actin cytoskeleton. Primary antibodies for integrin blocking were against β1 integrin (mAb13; from M. J. Humphries, University of Manchester), α2β1 (JA218 and Gi9; from M. J. Humphries, Manchester), α5 (mAb16; from M. J. Humphries, University of Manchester, UK), α8 (T-20; Santa Cruz Biotechnology), αv (Abcam17E6), αvβ3 (LM609 and 23C6, Millipore) and αvβ6 (10D5, Millipore). Anti-β-actin (mAbAC-74, Sigma-Aldrich) was used as a loading control for western blots. Anti-E-cadherin antibody (rabbit mAb 24E10), from Cell Signaling, was used at 1:1000 dilution for western blots. Other cell junction antibodies were against N-cadherin (Abcam 12221), E-cadherin (BD Biosciences, 610182), β-catenin (BD Biosciences, 610154), syndecan-4 (Santa Cruz 5G9, sc-12766) and PKCα (Abcam 57415).

siRNA transfections

Cells were transfected using lipofectamine RNAiMAX reagent (Life Technologies), according to the manufacturer's protocol. Briefly, 6 pmol RNAi duplex was added to 100 µl Optim-MEM medium (Life Technologies) prior to addition of 1 µl Lipofectamine RNAiMAX in a single well of a 24-well plate, with Lipofectamine RNAiMAX-only controls. The resulting solution was allowed to incubate for 15 minutes. HDFs, ARPE-19 cells or podocytes were trypsinised and counted prior to being diluted in DMEM (without antibiotics) so that 500 µl contained either 50,000 cells (HDF) or 75,000 cells (ARPE-19 cells and podocytes). The cells were then added to the transfection mix, giving a final RNAi duplex concentration of 10 nM. Cells were cultured for a total of up to 8 days (HDF) or 7 days (ARPE-19 and podocytes), with repeated RNAi duplex transfection taking place at regular intervals (day 2 for 4-day HDF; days 2, 4 and 7 for 8-day HDF; days 3 and 5 for ARPE-19 and podocytes). Depending on efficiency of knockdown, one or two RNAi duplexes were used per gene. The RNAi duplexes were: FN (SI02664004, Qiagen); EXT-1, 5′-GGAUCAUCCCAGGACAGGA-3′ and 5′-GGCUUAUUUUUCUUCAGUU-3′ (sense), (Busse et al., 2007); syndecan-2 (s12635/6, Ambion); syndecan-4 (s12638/9, Ambion); PKCα (SI00301308, Qiagen); perlecan (5′- GUUGGAGCAGCGGACAUAU-3′ (sense), (Sakai et al., 2009). DNA and RNA oligonucleotides were purchased from MWG Operon.

Immunofluorescence microscopy

ECM deposition was analyzed using indirect immunofluorescence microscopy. Cells cultured on coverslips were fixed using 4% (v/v) paraformaldehyde (PFA) solution for 20 minutes at room temperature, followed by washing in phosphate-buffered saline (PBS) and quenching in 0.2 M glycine for 20 minutes. Following three PBS washes, cells were permeabilised using 0.5% (v/v) Triton-X in PBS for 10 minutes at room temperature. Three PBS washes preceded blocking in 2% (w/v) fish-skin gelatin (Sigma-Aldrich) in PBS for 1 hour at room temperature. Coverslips were then incubated in primary antibody for 1 hour, before being washed in PBS and incubated in secondary antibody for 45 minutes (both incubations at room temperature). Coverslips were washed in dH_2O before being mounted on glass slides with Prolong Gold containing DAPI (Life Technologies). Primary antibodies (as above) were detected using Alexa Fluor secondary antibodies (1:400; Life Technologies) (see figure legends). Some cells were stained with phalloidin (as above). Images were collected at room temperature on an Olympus BX51 upright microscope using 20× or 60× objectives and captured using a Coolsnap ES camera (Photometrics) through MetaVue Software (Molecular Devices). Specific band pass filter sets for DAPI, FITC, Texas Red, Cy3 and Cy5 were used to prevent bleed through from one channel to the next. Images were processed and analyzed using ImageJ (http://rsb.info.nih.gov/ij).

Integrin, actomyosin and cadherin inhibition

ARPE-19 cells were cultured for 7 days in the presence of integrin blocking antibodies, all at 10 µg/ml, and ECM deposition was analyzed by indirect immunofluorescence microscopy (as above). ARPE-19 cells were also cultured in the presence of the myosin II inhibitor blebbistatin (10 µM), the Rho kinase inhibitor Y27632 (10 µM; Sigma-Aldrich), the RhoA activator lysophosphatidic acid (LPA) (20 µM), or cadherin inhibitor peptide (designated A7) (500 µM; Devemy and Blaschuk, 2009). Blebbistatin and Y27632 solutions contained DMSO; an equivalent concentration of DMSO was added to control cultures for these assays. All antibodies and inhibitors were added at day 0, and replenished at days 3 and 5.

Western blotting

Total cell lysates (from cultures up to 8 days) were prepared by incubation of cell layers in radio-immunoprecipitation assay buffer (RIPA buffer; 25 mM Tris-HCl pH 7.6, 150 mM NaCl, 1% (v/v) NP-40, 1% (v/v) sodium deoxycholate, 0.1% SDS; Thermo Scientific) for 15 minutes at room temperature, followed by cell scraping. Lysate concentrations were determined using a bicinchoninic acid (BCA) assay kit (Thermo Fisher Scientific). For SDS-PAGE separation of lysate proteins, 10 µg of total cell lysates were reduced with sample reducing agent (Invitrogen) before loading onto NuPAGE® Novex 3–8% Tris-acetate gels (Life Technologies). For samples of medium, 20 µl was reduced and loaded onto 3–8% Tris-acetate gels. For podocytes, soluble cell lysate was collected by addition of 1% (v/v) NP-40 for 1 minute at room temperature, before washing in PBS and addition of RIPA buffer, as above. The RIPA cell layer extract was centrifuged at 16,100 ***g*** for 30 minutes at 4℃. The supernatant ('soluble CL') was removed, and the pellet resuspended in 8 M urea ('insoluble CL'). Concentration determinations and SDS-PAGE analysis were as above. Separated proteins from gels were transferred onto nitrocellulose membranes prior to blocking in 5% (v/v) milk in TBST (150 mM NaCl, 10 mM Tris, 0.05% Tween-20). Blots were probed with anti-FN (mouse mAb FN-3E2, Sigma-Aldrich), anti-fibrillin-1 (HPA021057, Sigma-Aldrich), anti-PKCα (Abcam 57415) or anti-E-cadherin (rabbit mAb 24E10, Cell Signaling) antibodies overnight at 4℃. Blots were washed extensively in 2% (v/v) milk in TBST, and incubated for 1 hour at room temperature in goat anti-mouse-Ig or goat anti-rabbit-Ig antibodies conjugated to horseradish peroxidase (HRP) (Dako). Blots were washed extensively in TBST, and HRP detection performed using Super Signal Development Substrate (Pierce). To ensure equal loadings, total cell layer extract blots were stripped with western blot stripping buffer (Pierce), and re-probed with anti-β-actin antibody (see above). Band intensities were quantified using the Gene Tools software (Syngene).

Real-time quantitative PCR

RNA was isolated from ARPE-19, HDF cells and podocytes using an Absolute RNA Microprep Kit (Agilent Technologies). 500 ng RNA was used to generate cDNA using a cDNA synthesis kit (Bioline). Real-time qPCR analysis was carried out using either DNA Engine Opticon 2 (MJ Research Inc.) or CFX96/384 instruments (Bio-Rad) and the GoTaq qPCR Mastermix Kit (Promega). Expression analysis was performed in triplicate using CFX Manager software v3.0 (Bio-Rad), with samples normalised to a combination of TATA box binding protein (TBP) and glyceraldehyde 3-phosphate dehydrogenase (GAPDH) expression unless otherwise stated. Gene expression data (relative to control cell expression) from across replicate experiments was either entered directly into Prism software v4.03 (GraphPad Software Inc.) or (when stated in figure legends) first imported into the 'Gene Study' functionality of CFX Manager prior to transfer of expression, s.e.m., and *n*-values into Prism. Prism software was used for analysis via two-way ANOVA with Bonferroni post-tests. The oligonucleotide primers used for all qPCR reactions are shown in supplementary material Table S1.

TGFβ1 and cellular fibronectin incubations

ARPE-19 cells and podocytes were prepared for siRNA transfections as described above, and allowed to adhere for 4 hours prior to addition of human TGFβ1 (240-B-002, R&D Systems) to a final concentration of 160 pM. Cells were subject to repeat RNAi duplex transfections, together with addition of 160 pM TGFβ1, at days 3 and 5, and were cultured for 7 days in total. Immunofluorescence, RNA purification and real-time qPCR were performed as above. Similarly, siRNA knockdown ARPE-19B cells were allowed to adhere before addition of 10 µg/ml cellular

fibronectin (cFN; Sigma-Aldrich). Cells were cultured for 12 days, with repeat RNAi duplex transfection, together with cFN addition at days 3, 5, 7 and 10. Immunofluorescence was performed as above.

Electron microscopy of cell layers

ARPE-19 cells and podocytes were grown on Aclar film for 12 days (with repeated RNAi duplex transfection at day 0, 3, 5, 7 and 10, as above) prior to fixation with 2.5% glutaraldehyde and 4% paraformaldehyde in 0.1 M cacodylate buffer, postfixation with 1% osmium tetroxide for 1 hour, and treatement with 1% tannic acid for 1 hour and with 1% uranyl acetate for 1 hour. Samples were dehydrated with an alcohol series and embedded in TAAB LV resin. Ultrathin *en face* sections were cut at a Reichert Ultracut S Ultramicrotome and contrasted with lead citrate. Sections were observed with an FEI Tecnai Biotwin 12 microscope at 100 kV accelerating velocity.

Flow cytometry

Flow cytometry samples were prepared as described previously (Veevers-Lowe et al., 2011). Briefly, ARPE-19 cells were transfected with RNAi duplexes (see above), and cultured for 24 hours. Cells were trypsinised, and resuspended in medium prior to incubation at 37℃/5% CO_2 for 30 minutes to allow recovery of cell surface proteins. Following blocking with BSA (Sigma-Aldrich), phycoerythrin (PE)-conjugated anti-human CD29 (β1 integrin) antibody (MAR4; BD Biosciences), or syndecan-4 (Santa Cruz 5G9, sc-12766), was added to cells for 1 hour. Cells were extensively washed with PBS prior to incubation for 1 hour with 10 µg/ml Alexa-Fluor-488-cojugated anti-mouse-Ig antibody (syndecan-4 sample only; Life Technologies) followed by further extensive PBS washing and analysis on a Beckman Coulter Cyan ADP Analyzer.

Acknowledgements

We thank Rebecca Holley for her advice on EXT1 knockdown and HS antibodies, Clair Baldock for advice on manuscript preparation, Martin J. Humphries for integrin reagents, Christopher Ward and Sarah Ritson for the cadherin-blocking peptide and Aleksandr Mironov for electron microscopy support. The Faculty of Life Sciences Bioimaging Facility microscopes used in this study were funded by the Biotechnology and Biological Sciences Research Council (BBSRC) UK, the Wellcome Trust and University of Manchester Strategic Fund; we thank Dr Peter March and colleagues for microscopy support. Cell line authentication was carried out by Graeme Fox at the University of Manchester DNA Sequencing Facility.

Competing interests

The authors declare no competing interests.

Author contributions

A.K.B. conducted and analyzed the ARPE-19 cell experiments, including qPCR, protein analysis and immunomicroscopy, and prepared these data and figures. S.A.C. conducted the corresponding HDF experiments, and prepared these data and figures. R.L. provided the podocytes and advised on their biology. A.G. conducted electron microscopy. C.L.M. advised on the EXT1 and syndecan experiments, and manuscript. C.M.K. obtained the funding, led the study and wrote the manuscript.

Funding

This work was funded by the UK Medical Research Council [grant number G0801787 to C.M.K.]; and the Engineering and Physical Sciences Research Council, UK. Deposited in PMC for immediate release.

Supplementary material

Supplementary material available online at
http://jcs.biologists.org/lookup/suppl/doi:10.1242/jcs.134270/-/DC1

References

Baldwin, A. K., Simpson, A., Steer, R., Cain, S. A. and Kielty, C. M. (2013). Elastic fibres in health and disease. *Expert Rev. Mol. Med.* **15**, e8.

Bass, M. D., Morgan, M. R., Roach, K. A., Settleman, J., Goryachev, A. B. and Humphries, M. J. (2008). p190RhoGAP is the convergence point of adhesion signals from alpha 5 beta 1 integrin and syndecan-4. *J. Cell Biol.* **181**, 1013-1026.

Bass, M. D., Williamson, R. C., Nunan, R. D., Humphries, J. D., Byron, A., Morgan, M. R., Martin, P. and Humphries, M. J. (2011). A syndecan-4 hair trigger initiates wound healing through caveolin- and RhoG-regulated integrin endocytosis. *Dev. Cell* **21**, 681-693.

Bax, D. V., Bernard, S. E., Lomas, A., Morgan, A., Humphries, J., Shuttleworth, C. A., Humphries, M. J. and Kielty, C. M. (2003). Cell adhesion to fibrillin-1 molecules and microfibrils is mediated by alpha 5 beta 1 and alpha v beta 3 integrins. *J. Biol. Chem.* **278**, 34605-34616.

Bix, G., Fu, J., Gonzalez, E. M., Macro, L., Barker, A., Campbell, S., Zutter, M. M., Santoro, S. A., Kim, J. K., Höök, M. et al. (2004). Endorepellin causes endothelial cell disassembly of actin cytoskeleton and focal adhesions through alpha2beta1 integrin. *J. Cell Biol.* **166**, 97-109.

Boregowda, R. K., Krovic, B. M. and Ritty, T. M. (2012). Selective integrin subunit reduction disrupts fibronectin extracellular matrix deposition and fibrillin 1 gene expression. *Mol. Cell. Biochem.* **369**, 205-216.

Braga, V. M., Machesky, L. M., Hall, A. and Hotchin, N. A. (1997). The small GTPases Rho and Rac are required for the establishment of cadherin-dependent cell-cell contacts. *J. Cell Biol.* **137**, 1421-1431.

Busse, M., Feta, A., Presto, J., Wilén, M., Grønning, M., Kjellén, L. and Kusche-Gullberg, M. (2007). Contribution of EXT1, EXT2, and EXTL3 to heparan sulfate chain elongation. *J. Biol. Chem.* **282**, 32802-32810.

Cain, S. A., Morgan, A., Sherratt, M. J., Ball, S. G., Shuttleworth, C. A. and Kielty, C. M. (2006). Proteomic analysis of fibrillin-rich microfibrils. *Proteomics* **6**, 111-122.

Cain, S. A., Baldwin, A. K., Mahalingam, Y., Raynal, B., Jowitt, T. A., Shuttleworth, C. A., Couchman, J. R. and Kielty, C. M. (2008). Heparan sulfate regulates fibrillin-1 N- and C-terminal interactions. *J. Biol. Chem.* **283**, 27017-27027.

Cain, S. A., McGovern, A., Small, E., Ward, L. J., Baldock, C., Shuttleworth, A. and Kielty, C. M. (2009). Defining elastic fiber interactions by molecular fishing: an affinity purification and mass spectrometry approach. *Mol. Cell. Proteomics* **8**, 2715-2732.

Chen, H. C., Zhu, Y. T., Chen, S. Y. and Tseng, S. C. (2012). Wnt signaling induces epithelial-mesenchymal transition with proliferation in ARPE-19 cells upon loss of contact inhibition. *Lab. Invest.* **92**, 676-687.

Chung, C. Y. and Erickson, H. P. (1997). Glycosaminoglycans modulate fibronectin matrix assembly and are essential for matrix incorporation of tenascin-C. *J. Cell Sci.* **110**, 1413-1419.

Couchman, J. R. (2010). Transmembrane signaling proteoglycans. *Annu. Rev. Cell Dev. Biol.* **26**, 89-114.

Dallas, S. L., Sivakumar, P., Jones, C. J., Chen, Q., Peters, D. M., Mosher, D. F., Humphries, M. J. and Kielty, C. M. (2005). Fibronectin regulates latent transforming growth factor-beta (TGF beta) by controlling matrix assembly of latent TGF beta-binding protein-1. *J. Biol. Chem.* **280**, 18871-18880.

Debnath, J., Muthuswamy, S. K. and Brugge, J. S. (2003). Morphogenesis and oncogenesis of MCF-10A mammary epithelial acini grown in three-dimensional basement membrane cultures. *Methods* **30**, 256-268.

Devemy, E. and Blaschuk, O. W. (2009). Identification of a novel dual E- and N-cadherin antagonist. *Peptides* **30**, 1539-1547.

Dovas, A., Yoneda, A. and Couchman, J. R. (2006). PKCbeta-dependent activation of RhoA by syndecan-4 during focal adhesion formation. *J. Cell Sci.* **119**, 2837-2846.

Dunn, K. C., Aotaki-Keen, A. E., Putkey, F. R. and Hjelmeland, L. M. (1996). ARPE-19, a human retinal pigment epithelial cell line with differentiated properties. *Exp. Eye Res.* **62**, 155-169.

Dzamba, B. J., Keene, D. R., Isogai, Z., Charbonneau, N. L., Karaman-Jurukovska, N., Simon, M. and Sakai, L. Y. (2001). Assembly of epithelial cell fibrillins. *J. Invest. Dermatol.* **117**, 1612-1620.

Dzamba, B. J., Jakab, K. R., Marsden, M., Schwartz, M. A. and DeSimone, D. W. (2009). Cadherin adhesion, tissue tension, and noncanonical Wnt signaling regulate fibronectin matrix organization. *Dev. Cell* **16**, 421-432.

Esko, J. D. and Lindahl, U. (2001). Molecular diversity of heparan sulfate. *J. Clin. Invest.* **108**, 169-173.

Faivre, L., Gorlin, R. J., Wirtz, M. K., Godfrey, M., Dagoneau, N., Samples, J. R., Le Merrer, M., Collod-Beroud, G., Boileau, C., Munnich, A. et al. (2003). In frame fibrillin-1 gene deletion in autosomal dominant Weill-Marchesani syndrome. *J. Med. Genet.* **40**, 34-36.

Galante, L. L. and Schwarzbauer, J. E. (2007). Requirements for sulfate transport and the diastrophic dysplasia sulfate transporter in fibronectin matrix assembly. *J. Cell Biol.* **179**, 999-1009.

Gopal, S., Bober, A., Whiteford, J. R., Multhaupt, H. A., Yoneda, A. and Couchman, J. R. (2010). Heparan sulfate chain valency controls syndecan-4 function in cell adhesion. *J. Biol. Chem.* **285**, 14247-14258.

Hartner, A., Menendez-Castro, C., Cordasic, N., Marek, I., Volkert, G., Klanke, B., Rascher, W. and Hilgers, K. F. (2012). Tubulointerstitial de novo expression of the α8 integrin chain in a rodent model of renal fibrosis—a potential target for anti-fibrotic therapy? *PLoS ONE* **7**, e48362.

Haynes, S. L., Shuttleworth, C. A. and Kielty, C. M. (1997). Keratinocytes express fibrillin and assemble microfibrils: implications for dermal matrix organization. *Br. J. Dermatol.* **137**, 17-23.

Hopf, M., Göhring, W., Mann, K. and Timpl, R. (2001). Mapping of binding sites for nidogens, fibulin-2, fibronectin and heparin to different IG modules of perlecan. *J. Mol. Biol.* **311**, 529-541.

Huang, X. G., Chen, Y. Z., Zhang, Z. T., Wei, Y. T., Ma, H. Z., Zhang, T. and Zhang, S. C. (2013). Rac1 modulates the vitreous-induced plasticity of mesenchymal movement in retinal pigment epithelial cells. *Clin. Experiment. Ophthalmol.* **41**, 779-787.

Hubmacher, D., Sabatier, L., Annis, D. S., Mosher, D. F. and Reinhardt, D. P. (2011). Homocysteine modifies structural and functional properties of fibronectin and interferes with the fibronectin-fibrillin-1 interaction. *Biochemistry* **50**, 5322-5332.

Hynes, R. O. (2012). The evolution of metazoan extracellular matrix. *J. Cell Biol.* **196**, 671-679.
Johnson, M. S., Lu, N., Denessiouk, K., Heino, J. and Gullberg, D. (2009). Integrins during evolution: evolutionary trees and model organisms. *Biochim. Biophys. Acta* **1788**, 779-789.
Jovanovic, J., Takagi, J., Choulier, L., Abrescia, N. G., Stuart, D. I., van der Merwe, P. A., Mardon, H. J. and Handford, P. A. (2007). alphaVbeta6 is a novel receptor for human fibrillin-1. Comparative studies of molecular determinants underlying integrin-rgd affinity and specificity. *J. Biol. Chem.* **282**, 6743-6751.
Kalluri, R. and Weinberg, R. A. (2009). The basics of epithelial-mesenchymal transition. *J. Clin. Invest.* **119**, 1420-1428.
Kinsey, R., Williamson, M. R., Chaudhry, S., Mellody, K. T., McGovern, A., Takahashi, S., Shuttleworth, C. A. and Kielty, C. M. (2008). Fibrillin-1 microfibril deposition is dependent on fibronectin assembly. *J. Cell Sci.* **121**, 2696-2704.
Klass, C. M., Couchman, J. R. and Woods, A. (2000). Control of extracellular matrix assembly by syndecan-2 proteoglycan. *J. Cell Sci.* **113**, 493-506.
Lennon, R., Byron, A., Humphries, J. D., Randles, M. R., Carisey, A., Murphy, S., Knight, D., Brenchley, P. E. and Zent, T. and Humphries, M. J. (2013). Global analysis reveals the complexity of the human glomerular extracellular matrix. *J. Am. Soc. Nephrol.* doi: 10.1681/ASN.2013030233.
Li, H., Wang, H., Wang, F., Gu, Q. and Xu, X. (2011). Snail involves in the transforming growth factor β1-mediated epithelial-mesenchymal transition of retinal pigment epithelial cells. *PLoS ONE* **6**, e23322.
Loeys, B. L., Gerber, E. E., Riegert-Johnson, D., Iqbal, S., Whiteman, P., McConnell, V., Chillakuri, C. R., Macaya, D., Coucke, P. J., De Paepe, A. et al. (2010). Mutations in fibrillin-1 cause congenital scleroderma: stiff skin syndrome. *Sci. Transl. Med.* **2**, 23ra20.
Lomas, A. C., Mellody, K. T., Freeman, L. J., Bax, D. V., Shuttleworth, C. A. and Kielty, C. M. (2007). Fibulin-5 binds human smooth-muscle cells through alpha5beta1 and alpha4beta1 integrins, but does not support receptor activation. *Biochem. J.* **405**, 417-428.
Mahalingam, Y., Gallagher, J. T. and Couchman, J. R. (2007). Cellular adhesion responses to the heparin-binding (HepII) domain of fibronectin require heparan sulfate with specific properties. *J. Biol. Chem.* **282**, 3221-3230.
Masola, V., Gambaro, G., Tibaldi, E., Brunati, A. M., Gastaldello, A., D'Angelo, A., Onisto, M. and Lupo, A. (2012). Heparanase and syndecan-1 interplay orchestrates fibroblast growth factor-2-induced epithelial-mesenchymal transition in renal tubular cells. *J. Biol. Chem.* **287**, 1478-1488.
Massam-Wu, T., Chiu, M., Choudhury, R., Chaudhry, S. S., Baldwin, A. K., McGovern, A., Baldock, C., Shuttleworth, C. A. and Kielty, C. M. (2010). Assembly of fibrillin microfibrils governs extracellular deposition of latent TGF beta. *J. Cell Sci.* **123**, 3006-3018.
Melrose, J., Hayes, A. J., Whitelock, J. M. and Little, C. B. (2008). Perlecan, the "jack of all trades" proteoglycan of cartilaginous weight-bearing connective tissues. *Bioessays* **30**, 457-469.
Morgan, M. R., Hamidi, H., Bass, M. D., Warwood, S., Ballestrem, C. and Humphries, M. J. (2013). Syndecan-4 phosphorylation is a control point for integrin recycling. *Dev. Cell* **24**, 472-485.
Müller, U., Wang, D., Denda, S., Meneses, J. J., Pedersen, R. A. and Reichardt, L. F. (1997). Integrin alpha8beta1 is critically important for epithelial-mesenchymal interactions during kidney morphogenesis. *Cell* **88**, 603-613.
Nakajima, H. and Tanoue, T. (2011). Lulu2 regulates the circumferential actomyosin tensile system in epithelial cells through p114RhoGEF. *J. Cell Biol.* **195**, 245-261.
Nonaka, R., Onoue, S., Wachi, H., Sato, F., Urban, Z., Starcher, B. C. and Seyama, Y. (2009). DANCE/fibulin-5 promotes elastic fiber formation in a tropoelastin isoform-dependent manner. *Clin. Biochem.* **42**, 713-721.
Osterholm, C., Barczyk, M. M., Busse, M., Grønning, M., Reed, R. K. and Kusche-Gullberg, M. (2009). Mutation in the heparan sulfate biosynthesis enzyme EXT1 influences growth factor signaling and fibroblast interactions with the extracellular matrix. *J. Biol. Chem.* **284**, 34935-34943.
Ozbek, S., Balasubramanian, P. G., Chiquet-Ehrismann, R., Tucker, R. P. and Adams, J. C. (2010). The evolution of extracellular matrix. *Mol. Biol. Cell* **21**, 4300-4305.
Piha-Gossack, A., Sossin, W. and Reinhardt, D. P. (2012). The evolution of extracellular fibrillins and their functional domains. *PLoS ONE* **7**, e33560.
Ramirez, F. and Dietz, H. C. (2009). Extracellular microfibrils in vertebrate development and disease processes. *J. Biol. Chem.* **284**, 14677-14681.
Ramirez, F. and Sakai, L. Y. (2010). Biogenesis and function of fibrillin assemblies. *Cell Tissue Res.* **339**, 71-82.
Ritty, T. M., Broekelmann, T. J., Werneck, C. C. and Mecham, R. P. (2003). Fibrillin-1 and -2 contain heparin-binding sites important for matrix deposition and that support cell attachment. *Biochem. J.* **375**, 425-432.
Sabatier, L., Chen, D., Fagotto-Kaufmann, C., Hubmacher, D., McKee, M. D., Annis, D. S., Mosher, D. F. and Reinhardt, D. P. (2009). Fibrillin assembly requires fibronectin. *Mol. Biol. Cell* **20**, 846-858.
Sakai, K., Nakamura, T., Matsumoto, K. and Nakamura, T. (2009). Angioinhibitory action of NK4 involves impaired extracellular assembly of fibronectin mediated by perlecan-NK4 association. *J. Biol. Chem.* **284**, 22491-22499.
Saleem, M. A., O'Hare, M. J., Reiser, J., Coward, R. J., Inward, C. D., Farren, T., Xing, C. Y., Ni, L., Mathieson, P. W. and Mundel, P. (2002). A conditionally immortalized human podocyte cell line demonstrating nephrin and podocin expression. *J. Am. Soc. Nephrol.* **13**, 630-638.
Sato, Y., Shimono, C., Li, S., Nakano, I., Norioka, N., Sugiura, N., Kimata, K., Yamada, M. and Sekiguchi, K. (2013). Nephronectin binds to heparan sulfate proteoglycans via its MAM domain. *Matrix Biol.* **32**, 188-195.
Singh, P., Carraher, C. and Schwarzbauer, J. E. (2010). Assembly of fibronectin extracellular matrix. *Annu. Rev. Cell Dev. Biol.* **26**, 397-419.
Smith, A. L., Dohn, M. R., Brown, M. V. and Reynolds, A. B. (2012). Association of Rho-associated protein kinase 1 with E-cadherin complexes is mediated by p120-catenin. *Mol. Biol. Cell* **23**, 99-110.
Sottile, J. and Hocking, D. C. (2002). Fibronectin polymerization regulates the composition and stability of extracellular matrix fibrils and cell-matrix adhesions. *Mol. Biol. Cell* **13**, 3546-3559.
Stepp, M. A., Liu, Y., Pal-Ghosh, S., Jurjus, R. A., Tadvalkar, G., Sekaran, A., Losicco, K., Jiang, L., Larsen, M., Li, L. et al. (2007). Reduced migration, altered matrix and enhanced TGFbeta1 signaling are signatures of mouse keratinocytes lacking Sdc1. *J. Cell Sci.* **120**, 2851-2863.
Takahashi, S., Leiss, M., Moser, M., Ohashi, T., Kitao, T., Heckmann, D., Pfeifer, A., Kessler, H., Takagi, J., Erickson, H. P. et al. (2007). The RGD motif in fibronectin is essential for development but dispensable for fibril assembly. *J. Cell Biol.* **178**, 167-178.
Tamiya, S., Liu, L. and Kaplan, H. J. (2010). Epithelial-mesenchymal transition and proliferation of retinal pigment epithelial cells initiated upon loss of cell-cell contact. *Invest. Ophthalmol. Vis. Sci.* **51**, 2755-2763.
Terry, S. J., Zihni, C., Elbediwy, A., Vitiello, E., Leefa Chong San, I. V., Balda, M. S. and Matter, K. (2011). Spatially restricted activation of RhoA signalling at epithelial junctions by p114RhoGEF drives junction formation and morphogenesis. *Nat. Cell Biol.* **13**, 159-166.
Thiery, J. P. and Sleeman, J. P. (2006). Complex networks orchestrate epithelial-mesenchymal transitions. *Nat. Rev. Mol. Cell Biol.* **7**, 131-142.
Tian, J., Ishibashi, K., Honda, S., Boylan, S. A., Hjelmeland, L. M. and Handa, J. T. (2005). The expression of native and cultured human retinal pigment epithelial cells grown in different culture conditions. *Br. J. Ophthalmol.* **89**, 1510-1517.
Tiedemann, K., Bätge, B., Müller, P. K. and Reinhardt, D. P. (2001). Interactions of fibrillin-1 with heparin/heparan sulfate, implications for microfibrillar assembly. *J. Biol. Chem.* **276**, 36035-36042.
Tiedemann, K., Sasaki, T., Gustafsson, E., Göhring, W., Bätge, B., Notbohm, H., Timpl, R., Wedel, T., Schlötzer-Schrehardt, U. and Reinhardt, D. P. (2005). Microfibrils at basement membrane zones interact with perlecan via fibrillin-1. *J. Biol. Chem.* **280**, 11404-11412.
Tucker, R. P. and Chiquet-Ehrismann, R. (2009). Evidence for the evolution of tenascin and fibronectin early in the chordate lineage. *Int. J. Biochem. Cell Biol.* **41**, 424-434.
Veevers-Lowe, J., Ball, S. G., Shuttleworth, A. and Kielty, C. M. (2011). Mesenchymal stem cell migration is regulated by fibronectin through α5β1-integrin-mediated activation of PDGFR-β and potentiation of growth factor signals. *J. Cell Sci.* **124**, 1288-1300.
Wachi, H., Sato, F., Murata, H., Nakazawa, J., Starcher, B. C. and Seyama, Y. (2005). Development of a new in vitro model of elastic fiber assembly in human pigmented epithelial cells. *Clin. Biochem.* **38**, 643-653.
Woods, A., Longley, R. L., Tumova, S. and Couchman, J. R. (2000). Syndecan-4 binding to the high affinity heparin-binding domain of fibronectin drives focal adhesion formation in fibroblasts. *Arch. Biochem. Biophys.* **374**, 66-72.
Yamada, S. and Nelson, W. J. (2007). Localized zones of Rho and Rac activities drive initiation and expansion of epithelial cell-cell adhesion. *J. Cell Biol.* **178**, 517-527.
Yoneda, A., Ushakov, D., Multhaupt, H. A. and Couchman, J. R. (2007). Fibronectin matrix assembly requires distinct contributions from Rho kinases I and -II. *Mol. Biol. Cell* **18**, 66-75.
Zilberberg, L., Todorovic, V., Dabovic, B., Horiguchi, M., Couroussé, T., Sakai, L. Y. and Rifkin, D. B. (2012). Specificity of latent TGF-β binding protein (LTBP) incorporation into matrix: role of fibrillins and fibronectin. *J. Cell. Physiol.* **227**, 3828-3836.

Fig. S1. Microfibrils are not deposited by HDF cultures when FN is depleted. (A) Immunofluorescence microscopy of HDF cultures (8 days), showing deposition of fibrillin-1 (Fibr-1; B/W, red) and FN (B/W, green), with nuclei stained with DAPI (blue). Images were taken using a 20× objective. Specific band-pass filter sets for DAPI, FITC, and Cy3 or Cy5 were used to prevent bleed-through. Control cultures (Con) showed partial colocalisation of fibrillin-1 and FN (yellow). FN knockdown (kd) HDF cultures had no detectable microfibrils. EXT1 knockdown (kd) HDFs had disordered microfibrils but no apparent FN changes. Scale bars = 100 μm. n = 2 (B) Fibrillin-1 deposition was quantified using ImageJ. The percentage area was calculated by applying an equal threshold value over all the images and measuring the area of the brightest pixels corresponding to fibrillin fibrils. For each cell type, at least 3 images were used and the graph shows the mean percentage area and SEM. Statistical significance for deviation from the control cell-line values was calculated using a 2-way ANOVA with a Bonferroni's multiple comparisons test using GraphPad Prism V6. Asterisk indicate P values where *** = $P \leq 0.001$. (C) Medium and cell layer extracts from HDF cells in control (Con) and knockdown (kd) experiments (perlecan, EXT1, PKCα, FN, syndecan-2 or syndecan-4) were separated on 3-8% Tris-acetate gels in reducing conditions, and analyzed by western blotting for fibrillin-1 (antibody HPA021057) or FN (antibody FN-3E2), or β-actin (mAbAC-74) as loading control for cell layer extracts. Molecular weight markers are indicated. Quantification of band intensity is shown as a percentage of control band intensity (where Con = 100%). Data shown are from a single representative experiment, with biological and technical repeats exhibiting the same trends (n = 3).

Fig. S2. Relative expression levels in ARPE-19A and B cells, podocytes, and human dermal fibroblasts (HDFs). (A) Real-time quantitative PCR (qPCR) analysis of gene expression of fibrillin-1 (Fibr-1), fibronectin (FN), EXT1, perlecan (Perl), PKCα and syndecans (Syn) 1-4 in (i) ARPE-19A, (ii) ARPE-19B, (iii) podocyte (all 7 days) and (iv) HDF cultures (4 days). (B) Real-time qPCR analysis of gene expression of E-cadherin (E-cad), N-cadherin (N-cad), PDGF receptor-β (PDGFRβ), smooth muscle α-actin (SMA), SNAI1, SNAI2 and TWIST 1 in (i) ARPE-19A, (ii) ARPE-19B, and (iii) podocyte cultures (all 7 days). For both (A) and (B), expression is reported relative to TATA box binding protein (TBP), where TBP expression is equal to 1. Data are represented as the mean ± s.e.m. See Table S1 for details of n values for ARPE-19A and B cultures; for podocytes, n = 3; for HDF in (A) (iii), n = 6-12, depending on gene.

Fig. S3. Real-time quantitative PCR analysis of expression levels following knockdown of EXT1, perlecan, or fibronectin, and syndecan-2, syndecan-4 or PKCα. (A-D) qPCR analysis of expression levels of fibrillin-1 (Fibr-1), fibronectin (FN), EXT1, Perlecan (Perl), PKCα (PKCα) and syndecans (Syn) 1-4, following knockdown of EXT1, perlecan, or FN in (A) ARPE-19A, (B) ARPE-19B cells (both 7 days) and (C) HDF cultures (4 days). (D) qPCR analysis of expression levels of fibrillin-1 (Fibr-1), fibronectin (FN), syndecans (Syn) 1-4, E-cadherin (E-cad), N-cadherin (N-cad), PDGF receptor-β (PDGFRβ), smooth muscle α-actin (SMA), SNAI1, SNAI2 and TWIST 1 following knockdown of FN in podocyte cultures (7 days). Samples were either normalised to a combination of GAPDH/TBP expression (A, B and D), or to TBP expression (C) prior to being reported as fold changes relative to lipofectamine-treated control cell expression of either ARPE-19A, ARPE-19B, HDF or podocyte accordingly (where Con = 1). All data are represented as the mean ± s.e.m. and analyzed by 2-way ANOVA, with *P<0.05; **P<0.01; ***P<0.001. See Table S1 for details of n values for ARPE-19A and B cultures; for HDF, n = 3-16, depending on gene and knockdown condition. (E-H) qPCR analysis of expression levels of fibrillin-1 (Fibr-1), fibronectin (FN), EXT1, Perlecan (Perl), PKCα (PKCα) and syndecans (Syn) 1-4, following knockdown of syndecan-2, syndecan-4 or PKCα in (E) ARPE-19A, (F) ARPE-19B cells (both 7 days) and (G) HDF cultures (4 days). Samples were either normalised to a combination of GAPDH/TBP expression (E and F), or to TBP expression (G) prior to being reported as fold changes relative to lipofectamine-treated control cell expression of either ARPE-19A, ARPE-19B, or HDF accordingly (where Con = 1). All data are represented as mean ± s.e.m. and analyzed by 2-way ANOVA, with *P<0.05; **P<0.01; ***P<0.001. See Table S1 for details of n values for ARPE-19A and B cultures; for HDF, n = 3-16, depending on gene and knockdown condition. (H) Cell lysate samples of ARPE-19A and B cells (control and PKCα knockdown) were separated on 4-12% Bis-Tris gels in reducing conditions, and analyzed by western blotting for PKCα or β-actin (mAbAC-74) as loading control for cell layer extracts. Molecular weight markers are indicated. Verification of PKCα kd was achieved via quantification of band intensity ("Expression"), shown as a percentage of control band intensity (where Con = 100%).

Fig. S4. Effects of adding cellular fibronectin on microfibril and FN deposition by ARPE-19B cultures. Immunofluorescence microscopy of ARPE-19B cells (control and FN kd, 12 days), showing deposition of fibrillin-1 (Fibr-1; B/W, red) and FN (B/W, green), with nuclei stained with DAPI (blue), in the presence or absence of cellular FN (cFN; 10 μg/ml) . Addition of cFN to FN kd ARPE-19B cells failed to rescue deposition of fibrillin-1. Images were taken using a 20× objective. Specific band-pass filter sets for DAPI, FITC and Cy3 or Cy5 were used to prevent bleed-through. Scale bars = 100 μm.

Fig. S5. Effects on microfibrils of knocking down perlecan, or syndecans-2 or -4, or PKCα, in ARPE-19A, ARPE-19B and HDF cultures. Immunofluorescence microscopy of (A) ARPE-19A cells and (B) ARPE-19B cells (both 7 days), showing deposition of perlecan (B/W, red) and FN (B/W, green), with nuclei stained with DAPI (blue). Images were using a 20× objective. Boxed areas are shown as zoomed images on right. Control cultures (Con) showed partial colocalisation of fibronectin and perlecan (yellow). FN knockdown (kd) ARPE-19A cultures exhibited prominent perlecan staining, but FN knockdown ARPE-19B cultures had no detectable perlecan. Perlecan knockdown in both ARPE-19A and B cultures had no effect on FN deposition, and loss of perlecan was shown. Scale bars for first three lanes = 100 μm; scale bar for perlecan zoom = 25 μm; for A and B n = 3. (C) Immunofluorescence microscopy of HDF cultures (8 days), showing deposition of fibrillin-1 (Fibr-1; B/W, red) and perlecan (B/W, green), with nuclei stained with DAPI (blue). Boxed areas are shown as zoomed images on right. Control cultures (Con) showed partial colocalisation of fibrillin-1 and perlecan (yellow). FN knockdown (kd) HDFs had no detectable perlecan or microfibrils. Perlecan knockdown HDFs had some microfibrils. (D) Immunofluorescence microscopy of HDF cultures (8 days), showing deposition of fibrillin-1 (Fibr-1; B/W, red) and FN (B/W, green), with nuclei stained with DAPI (blue). Boxed areas are shown as zoomed images on right. PKCα, syndecan-2 and syndecan-4 knockdown (kd) HDFs had few microfibrils but abundant FN. For both (A) and (B), images were taken using a 20× objective. Scale bars = 100 μm, n = 3. For all microscopy, specific band-pass filter sets for DAPI, FITC, and Cy3 or Cy5 were used to prevent bleed-through.

Fig. S6. Real-time quantitative PCR analysis of syndecan and E-cadherin expression levels following siRNA treatments. qPCR analysis of expression levels of (A) syndecans 1-4 and (B) E-cadherin, following knockdown of EXT1, FN, perlecan, PKCα, syndecan-2 or syndecan-4 in ARPE-19A cells (black bars) and ARPE-19B cells (white bars; both 7 days). Samples were normalised to a combination of GAPDH/TBP expression prior to being reported as fold changes relative to ARPE-19A lipofectamine-treated control cell expression (where ARPE-19A Con = 1). E-cadherin expression is lower in control ARPE-19B cultures compared to control ARPE-19A cultures (see also Fig. 2). In both ARPE-19A and B cells, knockdown of EXT1 results in an increase in E-cadherin expression. None of the other gene knockdowns tested changed E-cadherin expression in ARPE-19B cells, whereas knockdown of perlecan and PKCα had consequences for E-cadherin expression in ARPE-19A cells. (C) Real-time quantitative PCR (qPCR) analysis of gene expression of syndecans 1-4 in control (Con) and FN kd ARPE-19A and B cells. For (A), (B) and (C), the "Gene Study" functionality of CFX Manager was utilised. In order to use the "Gene Study" software throughout the experiment, datasets were generated for ARPE-19A and B cells (for (A) and (C), n = 3-5, and for (B) n = 3-9, depending on the knockdown condition). All data are represented as the mean ± s.e.m. and analyzed by 2-way ANOVA, with **P*<0.05; ***P*<0.01; ****P*<0.001.

Fig. S7. Effects of actomyosin inhibitors and EXT1 knockdown on microfibril and FN deposition by ARPE-19A and B cultures. (A) Immunofluorescence microscopy of ARPE-19A and ARPE-19B cells (both cultured for 7 days), showing deposition of fibrillin-1 (Fibr-1; B/W, red) and FN (B/W, green), with nuclei stained with DAPI (blue). Images were taken using a 20× objective. ARPE-19A and B cells were incubated for 7 days in the presence of the myosin II inhibitor blebbistatin (10 μM), or the Rho kinase inhibitor Y27632 (10 μM), or the RhoA activator lysophosphatidic acid (LPA) (20 μM), with DMSO control cultures (DMSO). Microfibrils and FN were greatly reduced in both ARPE-19A and B cells by blebbistatin or Y27632, with only faint fine microfibril arrays observed. Scale bars for first three lanes = 100 μm; scale bar for Fibr-1 zoom = 25 μm. (B) Immunofluorescence microscopy of (i) ARPE-19A and (ii) ARPE-19B cells (both cultured for 7 days), showing deposition of fibrillin-1 (Fibr-1; B/W, red) and FN (B/W, green) after EXT1 knockdown (kd), with nuclei stained with DAPI (blue). Images were taken using a 20× objective. Control cultures (Con) showed partial colocalisation of fibrillin-1 and FN (yellow). EXT1 kd in both ARPE-19A and B cultures ablated microfibrils, with only cellular fibrillin-1 staining detected, and dense punctuate pericellular FN. Scale bars = 100 μm. For A, n = 2, and B, n = 4. For all microscopy, specific band-pass filter sets for DAPI, FITC, and Cy 3 or Cy5 were used to prevent bleed-through. Boxed areas are shown as zoomed images on right.

Fig. S1

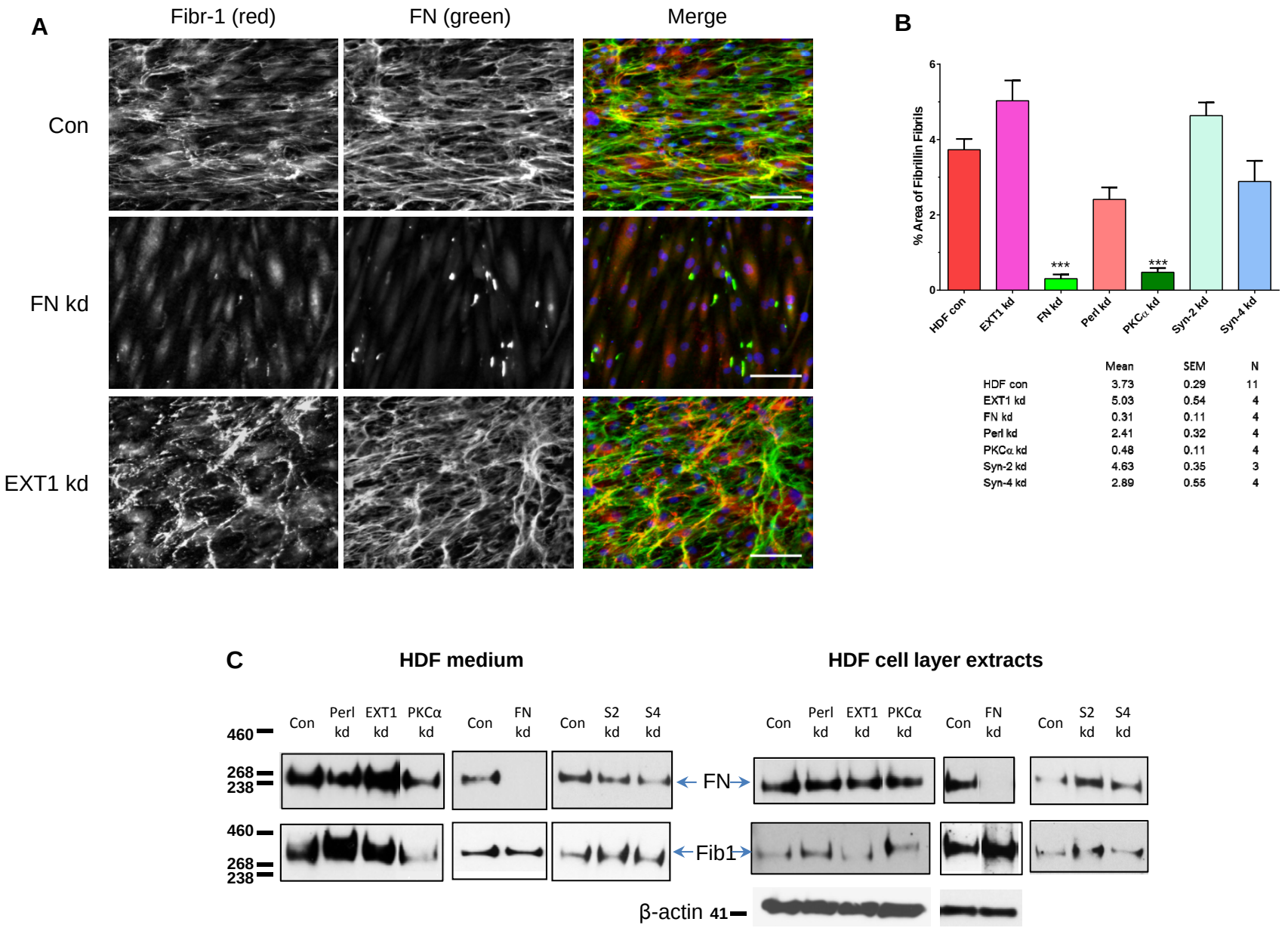
A
Fibr-1 (red)
FN (green)
Merge
Con
FN kd
EXT1 kd
B
% Area of Fibrillin Fibrils
6
4
2
0
***
***
HDF con
EXT1 kd
FN kd
Perl kd
PKCα kd
Syn-2 kd
Syn-4 kd
Mean SEM N
HDF con 3.73 0.29 11
EXT1 kd 5.03 0.54 4
FN kd 0.31 0.11 4
Perl kd 2.41 0.32 4
PKCα kd 0.48 0.11 4
Syn-2 kd 4.63 0.35 3
Syn-4 kd 2.89 0.55 4
C
HDF medium
HDF cell layer extracts
Con
Perl kd
EXT1 kd
PKCα kd
Con
FN kd
Con
S2 kd
S4 kd
460
268
238
FN
Fib1
β-actin 41

Fig. S2

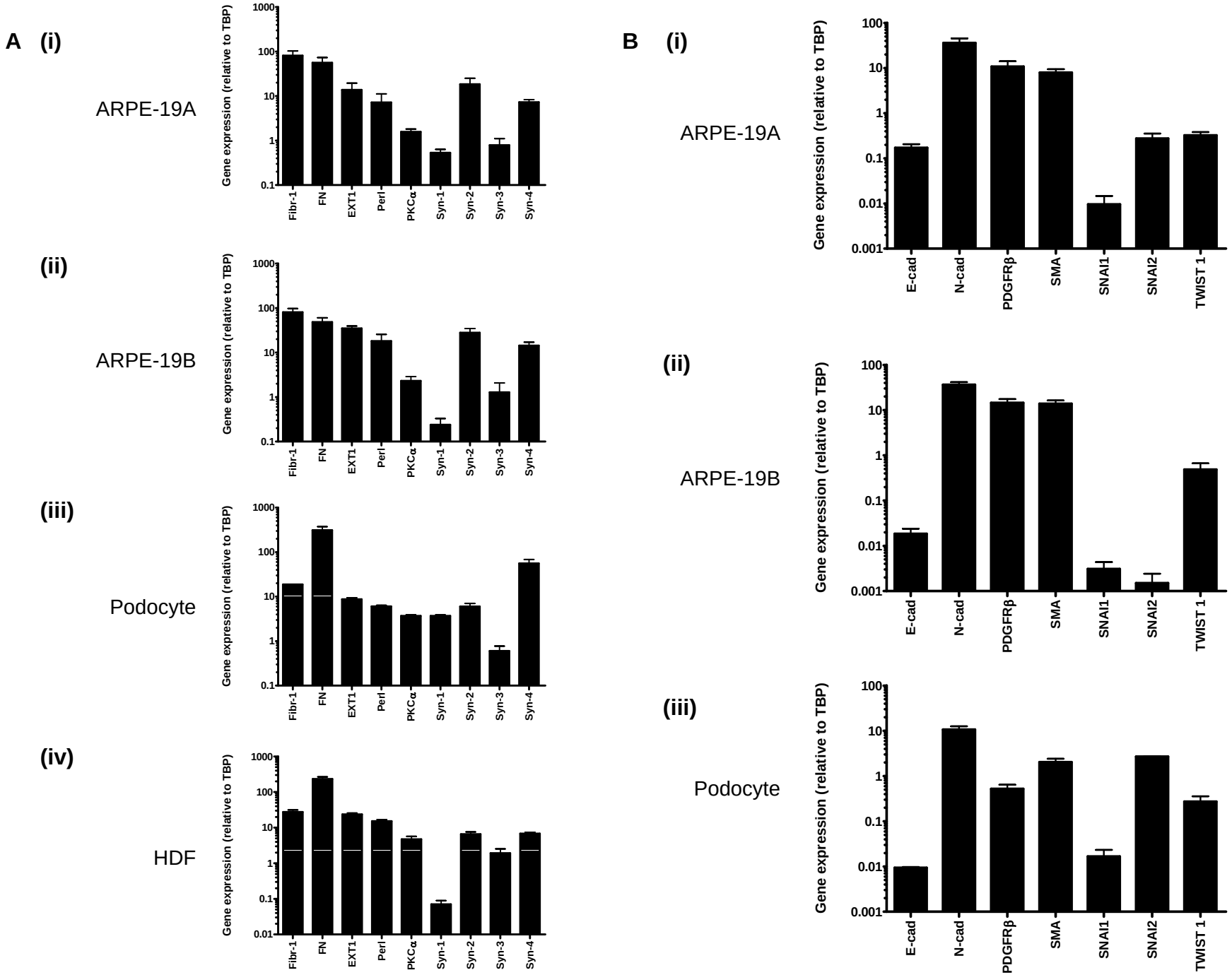
A
(i)
ARPE-19A
(ii)
ARPE-19B
(iii)
Podocyte
(iv)
HDF
Gene expression (relative to TBP)
Fibr-1
FN
EXT1
Perl
PKCα
Syn-1
Syn-2
Syn-3
Syn-4
B
(i)
ARPE-19A
(ii)
ARPE-19B
(iii)
Podocyte
Gene expression (relative to TBP)
E-cad
N-cad
PDGFRβ
SMA
SNAI1
SNAI2
TWIST 1

Fig. S3

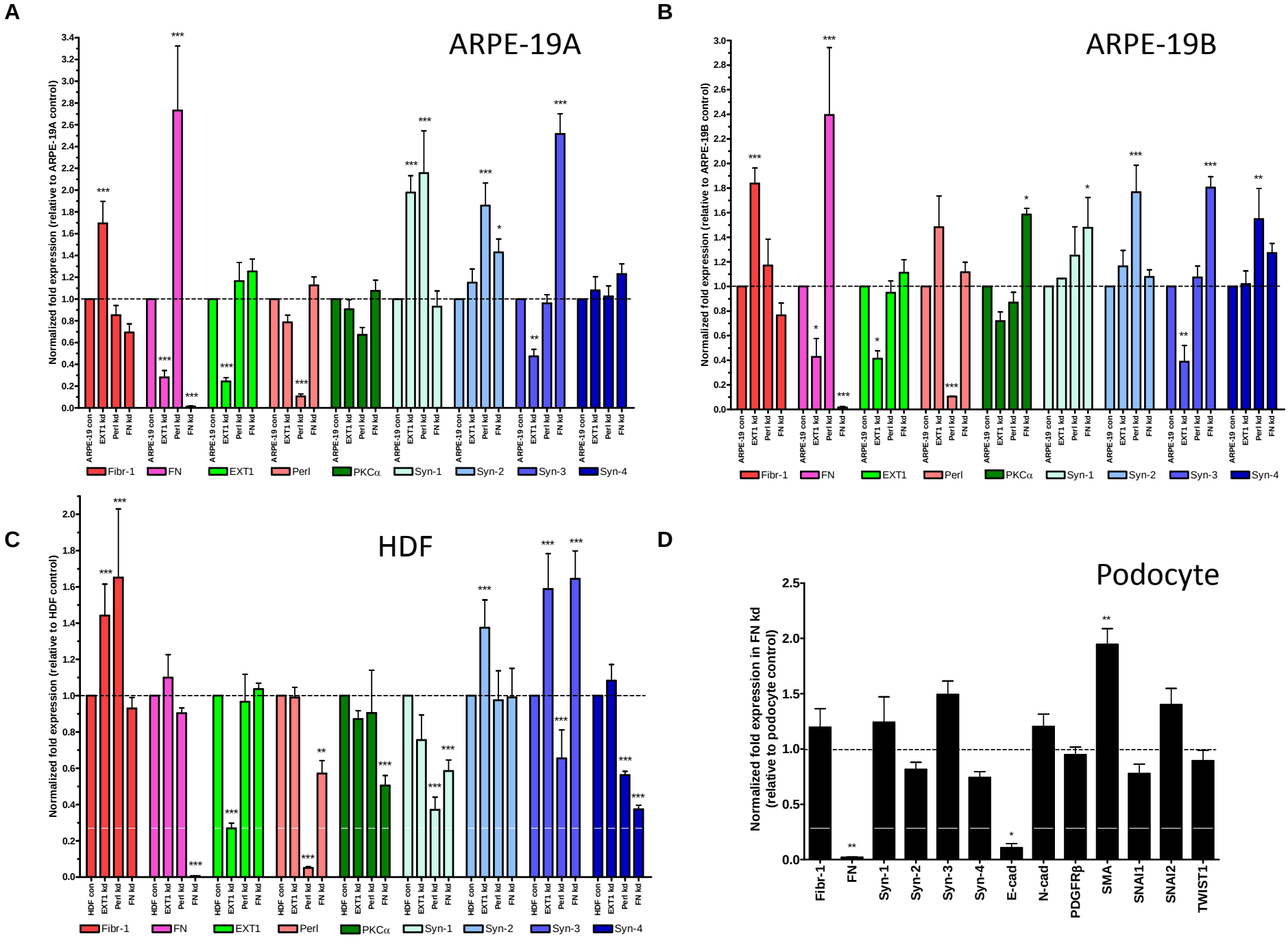
A
ARPE-19A
Normalized fold expression (relative to ARPE-19A control)
B
ARPE-19B
Normalized fold expression (relative to ARPE-19B control)
C
HDF
Normalized fold expression (relative to HDF control)
D
Podocyte
Normalized fold expression in FN kd (relative to podocyte control)
ARPE-19 con
HDF con
EXT1 kd
Perl kd
FN kd
Fibr-1
FN
EXT1
Perl
PKCα
Syn-1
Syn-2
Syn-3
Syn-4
Fibr-1
FN
Syn-1
Syn-2
Syn-3
Syn-4
E-cad
N-cad
PDGFRβ
SMA
SNAI1
SNAI2
TWIST1

Fig. S3

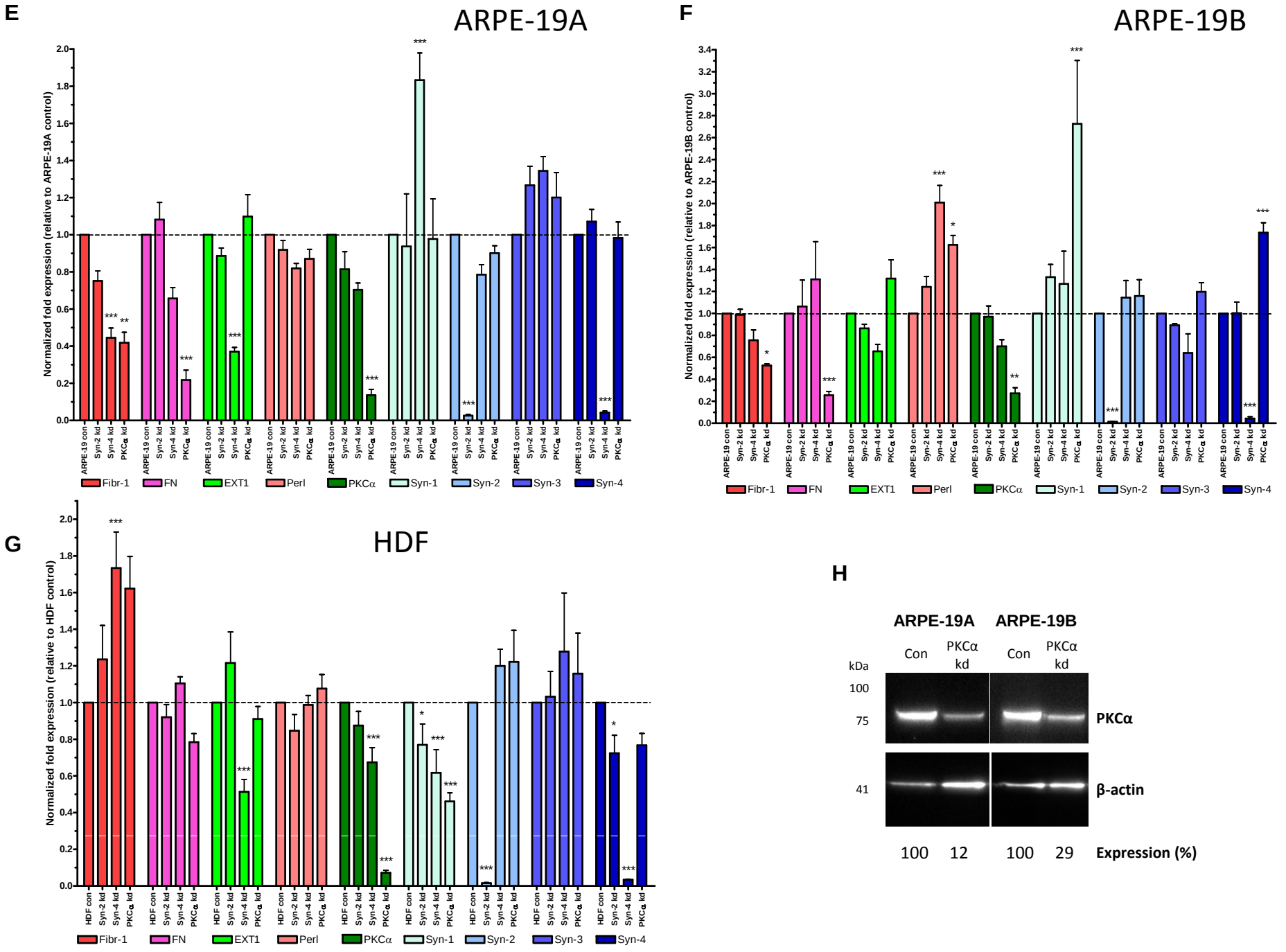
E
ARPE-19A
Normalized fold expression (relative to ARPE-19A control)
F
ARPE-19B
Normalized fold expression (relative to ARPE-19B control)
ARPE-19 con
Syn-2 kd
Syn-4 kd
PKCα kd
Fibr-1
FN
EXT1
Perl
PKCα
Syn-1
Syn-2
Syn-3
Syn-4
G
HDF
Normalized fold expression (relative to HDF control)
HDF con
H
ARPE-19A
ARPE-19B
Con
PKCα kd
kDa
100
75
41
PKCα
β-actin
100
12
100
29
Expression (%)

Fig. S4

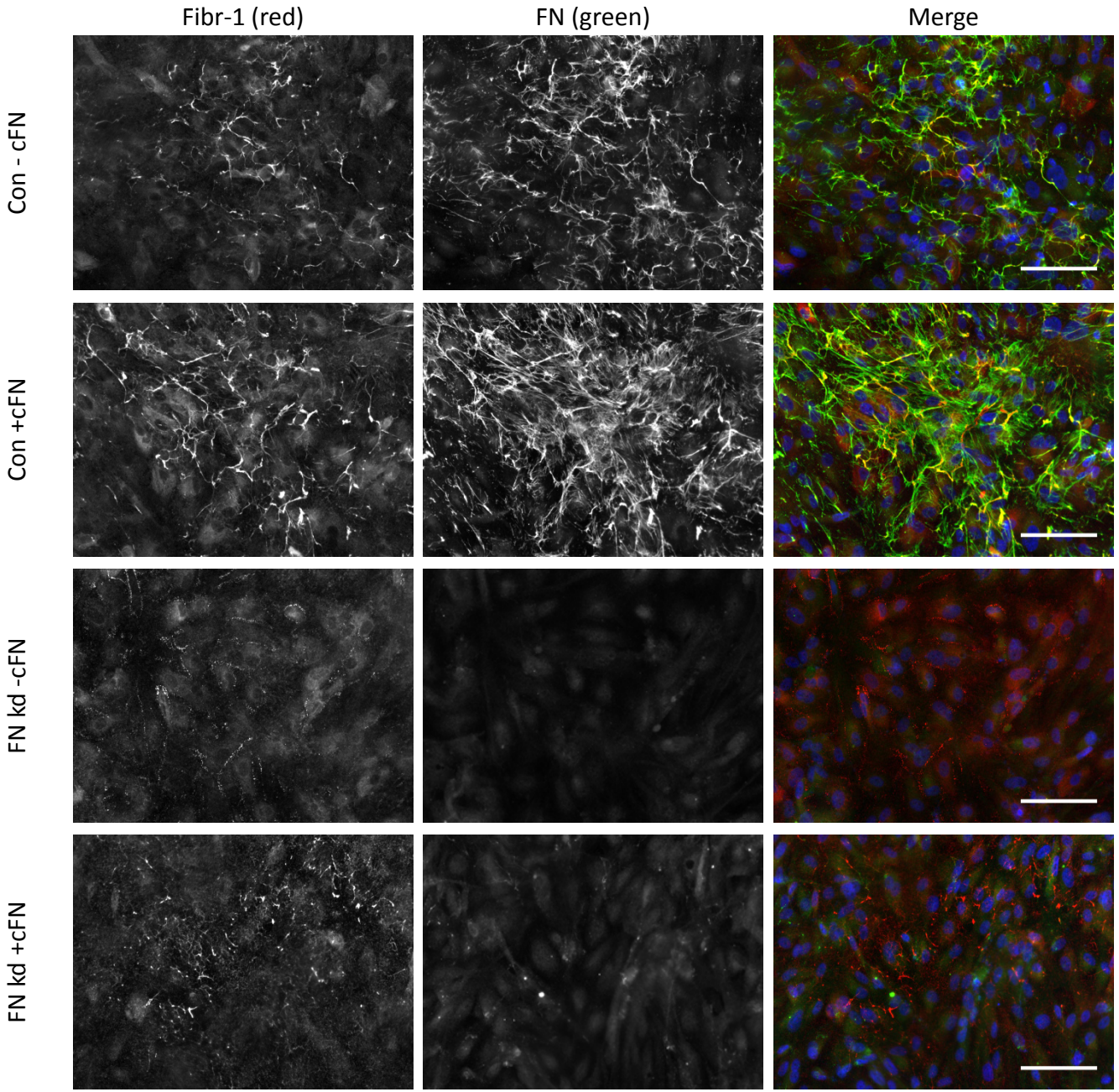

Fig. S5

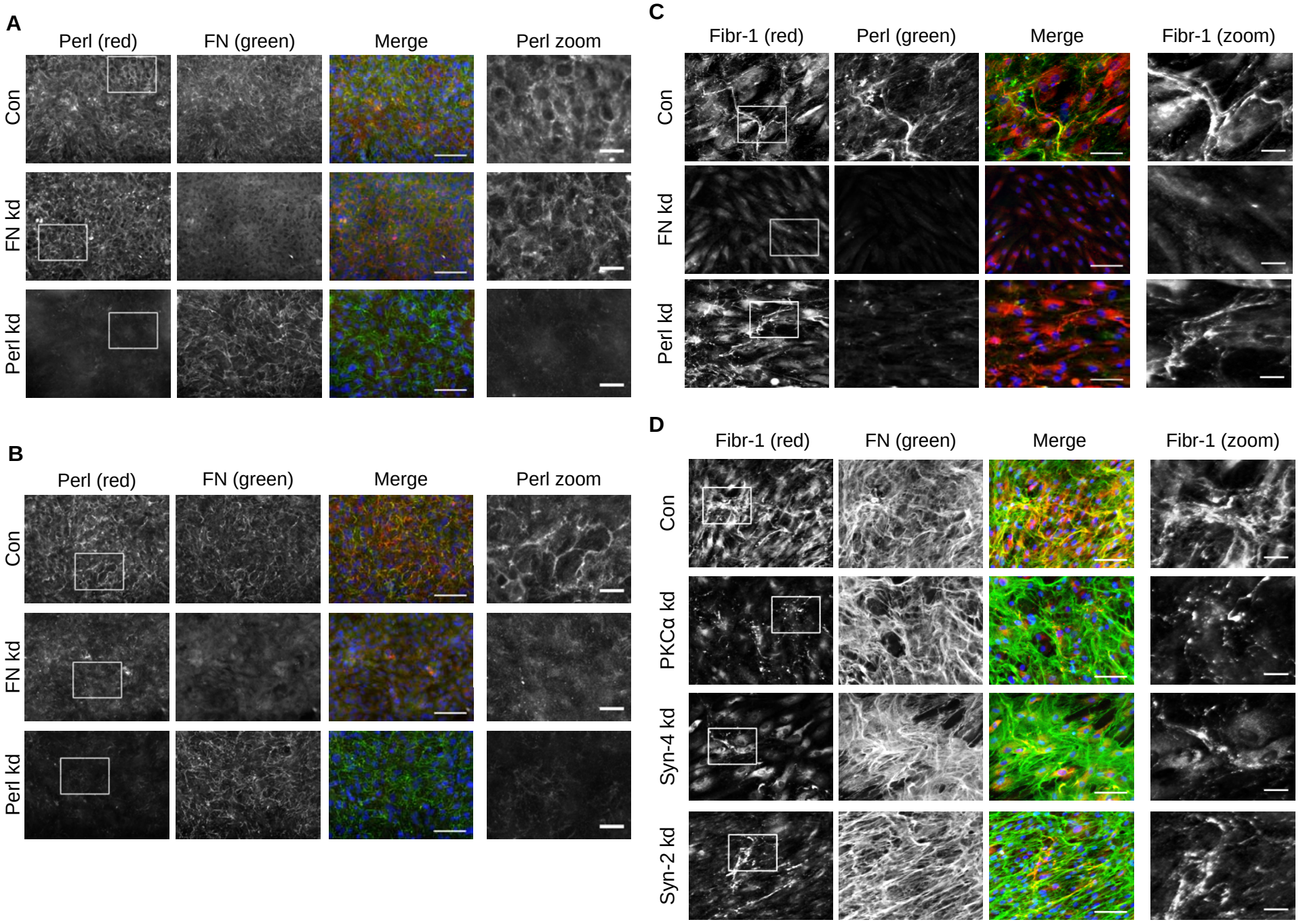
A
Perl (red)
FN (green)
Merge
Perl zoom
Con
FN kd
Perl kd
B
Perl (red)
FN (green)
Merge
Perl zoom
Con
FN kd
Perl kd
C
Fibr-1 (red)
Perl (green)
Merge
Fibr-1 (zoom)
Con
FN kd
Perl kd
D
Fibr-1 (red)
FN (green)
Merge
Fibr-1 (zoom)
Con
PKCα kd
Syn-4 kd
Syn-2 kd

Fig. S6

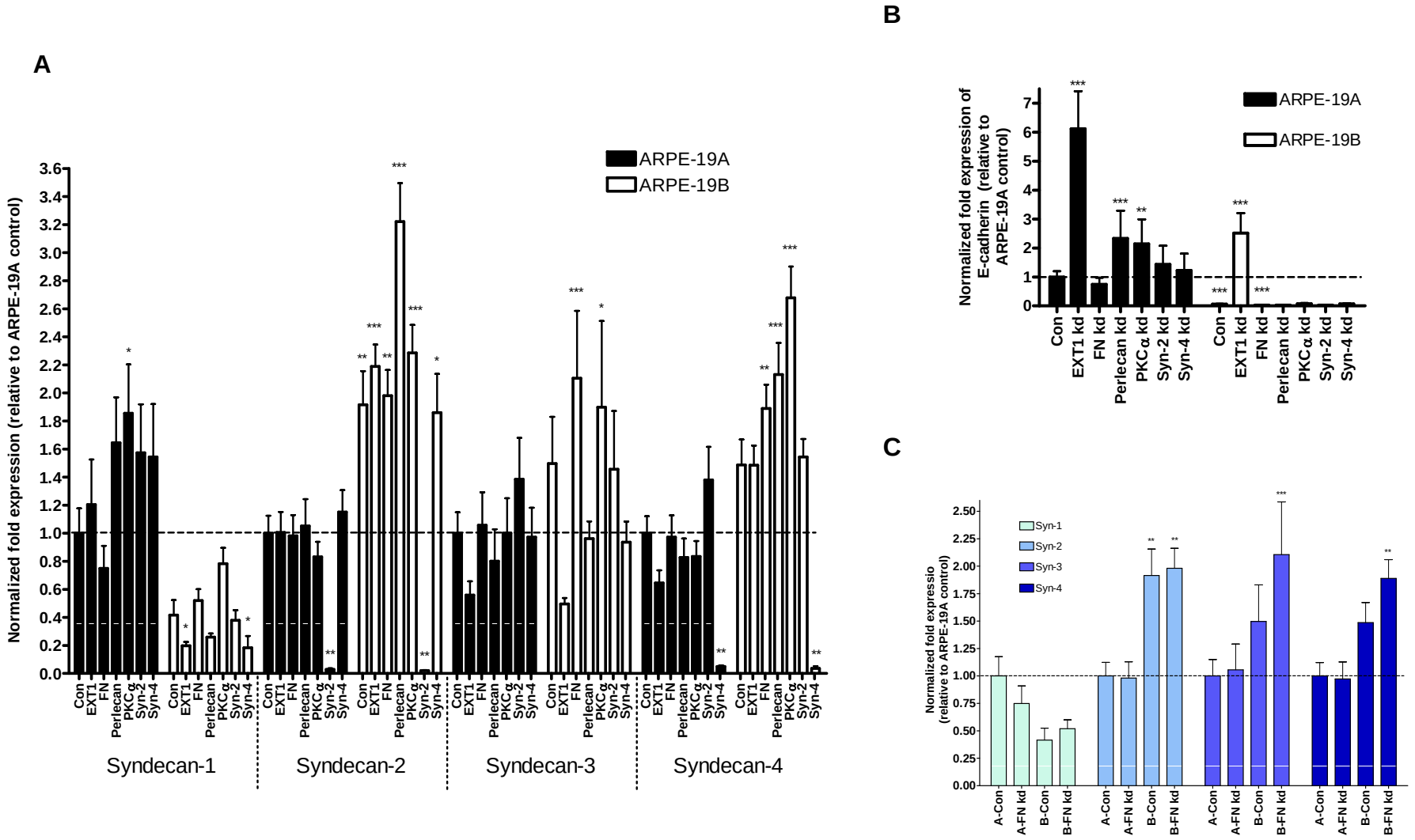
A
ARPE-19A
ARPE-19B
Normalized fold expression (relative to ARPE-19A control)
Con
EXT1
FN
Perlecan
PKCα
Syn-2
Syn-4
Syndecan-1
Syndecan-2
Syndecan-3
Syndecan-4
B
Normalized fold expression of E-cadherin (relative to ARPE-19A control)
ARPE-19A
ARPE-19B
Con
EXT1 kd
FN kd
Perlecan kd
PKCα kd
Syn-2 kd
Syn-4 kd
C
Normalized fold expressio (relative to ARPE-19A control)
Syn-1
Syn-2
Syn-3
Syn-4
A-Con
A-FN kd
B-Con
B-FN kd

Fig. S7

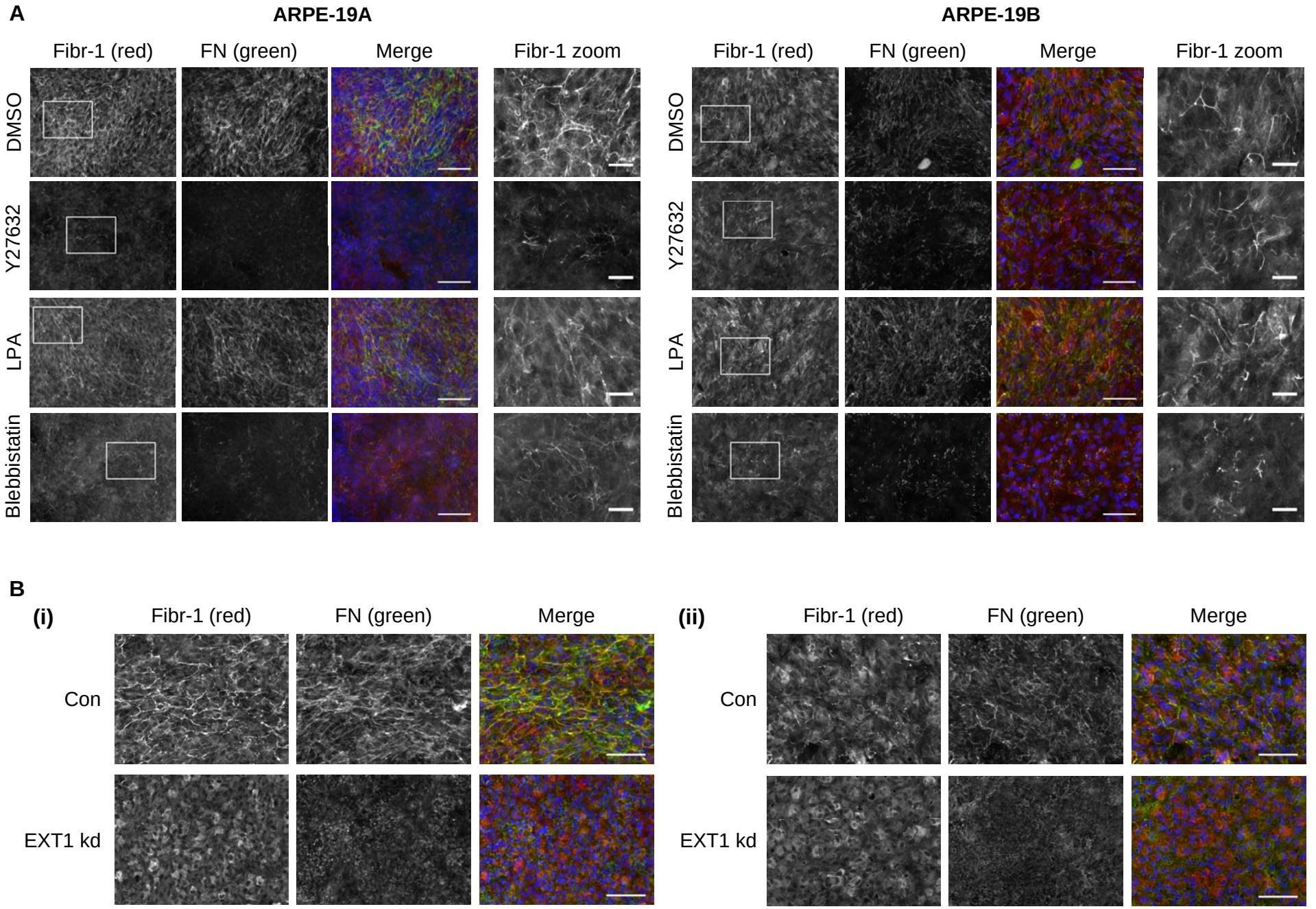
A
ARPE-19A
ARPE-19B
Fibr-1 (red)
FN (green)
Merge
Fibr-1 zoom
DMSO
Y27632
LPA
Blebbistatin
B
(i)
(ii)
Con
EXT1 kd

Table S1. Oligonucleotide primers used for qPCR analyses.

	Forward Primer (5′ – 3′)	**Reverse Primer (5′ – 3′)**
EXT1	GCTCTTGTCTCGCCCTTTTGT	TGGTGCAAGCCATTCCTACC
FN	CTGCGAGAGCAAACCTGAAG	TTTAGGACGCTCATAAGTGTCAC
TBP	TCGTGCCCGAAACGCCGAAT	CAGTGCCGTGGTTCGTGGCT
GAPDH	AAGGGCATCCTGGGCTAC	GTGGAGGAGTGGGTGTCG
PKCα	TGACGTGGAGTGCACCAT	GAGTGCAGCTGCGTCAAG
Fibrillin-1	GGGCATTTGCCAGAACAC	CGCTGAGGCATTCGTTTT
Syndecan-1	CCAGCCAAGCTGACCTTC	GAGGCTCCATCCTCAGCA
Syndecan-2	CCTGCTGTTGGTGTATCG	GCAGCACTGGATGGTTTG
Syndecan-3	GGAGCCTGACATCCCTGA	GGGGTCTGAGCCACCTCT
Syndecan-4	ACTGTGCAGGGCAGCAAC	AAGAGGATGCCCACGATG
Perlecan	TGCGCTGGACACATTCGTACCT	CCACTGCCCAGGTCGTCTCCT
E-cadherin	CATGAGCCACTGCACCTG	GCGATGGAGCGAAACTGT
N-cadherin	AATGACCCCACAGCTCCA	GAGCTCAAGGACCCAGCA
SMA	CATCACCAACTGGGACGA	GGTGGGATGCTCTTCAGG
PDGFRβ	CTCGGGGACCTACACCTG	ACGTAGCCGCTCTCAACC
SNAIL 1	TCCCATGGCCATTTCTGT	GACAGGCCAGCTCAGGAA
SNAIL 2	ACCCAATGGCCTCTCTCC	AGCCACTGTGGTCCTTGG
TWIST 1	ACCCAGTCGCTGAACGAG	GCCAGCTTGAGGGTCTGA

Publication: Journal of Cell Science (UK spelling)
Type: Research Article; Open Access: F; Volume: ; Issue:

Table S2. Total number of replicates for ARPE-19A and B qPCR studies. Table displaying the number of replicate experiments (n) performed in triplicate with ARPE-19A and B cells (7 days) to compile real-time quantitative PCR data. Values consist of a combination of technical and biological repeats. NA - not included in this study.

	ARPE-19A							ARPE-19B						
	Con	EXT1 kd	Perl kd	FN kd	Syn-2 kd	Syn-4 kd	PKCα kd	Con	EXT1 kd	Perl kd	FN kd	Syn-2 kd	Syn-4 kd	PKCα kd
Gene														
Fibr-1	10	5	4	5	7	7	4	11	3	3	10	3	3	3
FN	10	5	4	5	7	7	4	11	3	3	10	3	3	3
EXT1	6	6	4	6	5	6	3	4	3	3	3	3	3	3
Perlecan	5	4	5	4	4	4	4	4	3	3	3	3	3	3
PKCα	5	4	5	4	5	4	5	3	3	3	3	3	3	3
Syn-1	6	4	4	6	4	3	3	4	3	3	4	3	3	3
Syn-2	8	5	5	6	7	8	6	5	4	4	4	4	4	4
Syn-3	6	4	4	6	4	4	4	4	3	3	4	3	3	3
Syn-4	9	5	4	7	9	9	3	5	4	4	4	4	4	4
E-cad	12	3	3	9	3	3	3	11	3	3	8	3	3	3
N-cad	10	NA	NA	NA	NA	NA	NA	10	NA	NA	NA	NA	NA	NA
PDGFRβ	9	NA	NA	NA	NA	NA	NA	8	NA	NA	NA	NA	NA	NA
SMA	10	NA	NA	NA	NA	NA	NA	10	NA	NA	NA	NA	NA	NA
SNAI1	8	NA	NA	NA	NA	NA	NA	8	NA	NA	NA	NA	NA	NA
SNAI2	8	NA	NA	NA	NA	NA	NA	8	NA	NA	NA	NA	NA	NA
TWIST 1	7	NA	NA	NA	NA	NA	NA	7	NA	NA	NA	NA	NA	NA

	ARPE-19A							ARPE-19B						
	Con	EXT1 kd	Perl kd	FN kd	Syn-2 kd	Syn-4 kd	PKCα kd	Con	EXT1 kd	Perl kd	FN kd	Syn-2 kd	Syn-4 kd	PKCα kd
Gene														
Fibr-1	10	5	4	5	7	7	4	11	3	3	10	3	3	3
FN	10	5	4	5	7	7	4	11	3	3	10	3	3	3
EXT1	6	6	4	6	5	6	3	4	3	3	3	3	3	3
Perlecan	5	4	5	4	4	4	4	4	3	3	3	3	3	3
PKCα	5	4	5	4	5	4	5	3	3	3	3	3	3	3
Syn-1	6	4	4	6	4	3	3	4	3	3	4	3	3	3
Syn-2	8	5	5	6	7	8	6	5	4	4	4	4	4	4
Syn-3	6	4	4	6	4	4	4	4	3	3	4	3	3	3
Syn-4	9	5	4	7	9	9	3	5	4	4	4	4	4	4
E-cad	12	3	3	9	3	3	3	11	3	3	8	3	3	3
N-cad	10	NA	NA	NA	NA	NA	NA	10	NA	NA	NA	NA	NA	NA
PDGFRβ	9	NA	NA	NA	NA	NA	NA	8	NA	NA	NA	NA	NA	NA
SMA	10	NA	NA	NA	NA	NA	NA	10	NA	NA	NA	NA	NA	NA
SNAI1	8	NA	NA	NA	NA	NA	NA	8	NA	NA	NA	NA	NA	NA
SNAI2	8	NA	NA	NA	NA	NA	NA	8	NA	NA	NA	NA	NA	NA
TWIST 1	7	NA	NA	NA	NA	NA	NA	7	NA	NA	NA	NA	NA	NA